An Optimized Screen Reduces the Number of GA Transporters and provides Insights into NPF Substrate Determinants

1 **Nikolai Wulff[1], Heidi Asschenfeldt Ernst[2], Morten Egevang Jørgensen[1,3], Sophie Lambertz[1],**
2 **Tobias Maierhofer[3], Zeinu Mussa Belew[1], Christoph Crocoll[1], Mohammed Saddik Motawia[4]**
3 **Dietmar Geiger[3], Flemming Steen Jørgensen[2], Osman Mirza[2], Hussam Hassan Nour-Eldin[1*]**

4 [1]DynaMo Center, Copenhagen Plant Science Centre, Department of Plant and Environmental
5 Sciences, University of Copenhagen, Frederiksberg, Denmark. [2]Department of Drug Design and
6 Pharmacology, University of Copenhagen, Copenhagen, Denmark. [3]Julius-von-Sachs-Institute,
7 Molecular Plant Physiology and Biophysics, University Würzburg, Würzburg, Germany. [4]Center for
8 Plant Plasticity, Department of Plant and Environmental Sciences, University of Copenhagen,
9 Frederiksberg, Denmark

10

11 *** Correspondence:**
12 Hussam Hassan Nour-Eldin
13 Huha@plen.ku.dk

14 **Keywords: gibberellic acid$_1$, transport$_2$, NPF$_3$, membrane permeable$_4$, phytohormones$_5$, in**
15 **vitro$_6$, pH$_7$.**

16

17 **Abstract**

18 Based on recent *in vitro* data, a relatively large number of the plant Nitrate transporter 1/Peptide
19 transporter Family (NPF) proteins has been suggested to function as gibberellic acid (GA)
20 transporters. Most GA transporting NPF proteins also appear to transport other structurally unrelated
21 phytohormones or metabolites. Several of the GAs used in previous *in vitro* assays are membrane
22 permeable weak organic acids whose movement across membranes are influenced by the pH-
23 sensitive ion-trap mechanism. Moreover, a large proportion of *in vitro* GA transport activities have
24 been demonstrated indirectly via long-term yeast-based GA-dependent growth assays that are limited
25 to detecting transport of bioactive GAs. Thus, there is a need for an optimized transport assay for
26 identifying and characterizing GA transport. Here, we develop an improved transport assay in
27 *Xenopus laevis* oocytes wherein we directly measure movement of six different GAs across oocyte
28 membranes over short time. We show that membrane permeability of GAs in oocytes can be
29 predicted based on number of oxygen atoms and that several GAs do not diffuse over membranes
30 regardless of changes in pH values. In addition, we show that small changes in internal cellular pH
31 can result in strongly altered distribution of membrane permeable phytohormones. This prompts
32 caution when interpreting heterologous transport activities. We use our transport assay to screen all
33 *Arabidopsis thaliana* NPF proteins for transport activity towards six GAs (two membrane permeable
34 and four non-permeable). The results presented here, significantly reduce the number of *bona fide*
35 NPF GA transporters in *Arabidopsis* and narrow the activity to fewer subclades within the family.
36 Furthermore, to gain first insight into the molecular determinants of substrate specificities towards
37 organic molecules transported in the NPF, we charted all surface exposed amino acid residues in the
38 substrate-binding cavity and correlated them to GA transport. This analysis identified distinct

39 residues within the substrate-binding cavity that are shared between GA transporting NPF proteins;
40 the potential roles of these residues in determining substrate specificity are discussed.

41

1   Introduction

43 GAs were detected in phloem sap more than 50 years ago suggesting that GAs are mobile
44 phytohormones (Hoad and Bowen, 1968). This has since been supported by multiple studies
45 indicating that GAs can move long distances *in planta* and that transport processes generate local
46 concentration maxima that may be essential for the regulatory roles of GA (Regnault et al.,
47 2015;Regnault et al., 2016;Binenbaum et al., 2018). However, due to lack of molecular knowledge
48 on GA transport, the physiological role of GA mobility remains unclear.

49 Within recent years, novel *in vitro* and *in vivo* approaches led to the identification of a large number
50 of putative GA transporters (>25 different genes in *Arabidopsis* summarized in (Supplementary
51 Table 1). The majority of these genes belong to the NPF (Kanno et al., 2012;Chiba et al., 2015;Saito
52 et al., 2015;Tal et al., 2016). The physiological roles of two NPF-GA transporters have been
53 investigated *in planta*, namely NPF3.1 and NPF2.10 (Saito et al., 2015;David et al., 2016;Tal et al.,
54 2016). The GA related phenotypes in plants mutated in these genes are limited compared with those
55 observed in GA-deficient or GA signaling mutants (Sun, 2008;Plackett et al., 2011). The relatively
56 large number of potential NPF-GA transporters implies that there may be widespread functional
57 redundancy among these transporters. Accordingly, experiments in which expression of multiple
58 GA transporting NPF members are inhibited or knocked-out simultaneously may be needed to
59 unveil their distinct roles (Binenbaum et al., 2018).

60 The NPF proteins are plant specific subfamily members of the Proton-coupled Oligopeptide
61 Transporter (POT) family, which exists in all kingdoms of life and whose members are important for
62 transport of di- and tripeptides across membranes in symport with at least one proton. In humans,
63 there are four POT family members, two of which are prime targets for drug delivery owing to their
64 central importance for delivery of peptidomimetic drugs to intestinal epithelial cells (Daniel and
65 Kottra, 2004). Crystal structures of bacterial POT family members have identified key residues in the
66 POT substrate-binding cavity which interact with the peptidomimetic substrates and are located in a
67 large cavity able to accommodate nearly limitless variations in amino acid side chains and conjugated
68 species (Biegel et al., 2006;Doki et al., 2013;Guettou et al., 2014;Lyons et al., 2014;Newstead,
69 2015;2017). Moreover, a conserved ExxE[K/R] motif plays an essential role in intra-transporter salt
70 bridge formations that enable coupling between proton and substrate transport to ensure active
71 transport (Solcan et al., 2012;Aduri et al., 2015).

72 In *Arabidopsis*, 53 NPF members exist, which are divided into 8 distinct subclades (Léran et al.,
73 2014). Low affinity nitrate transport activities have been demonstrated in members from subclades 1,
74 2, 3, 4, 5, 6 and 7; peptide transport in subclades 5 and 8; glucosinolate transport in subclade 2; and
75 transport of the phytohormones abscisic acid (ABA), GA and jasmonoyl-isoleucine (JA-Ile) transport
76 activities have been demonstrated for members from subclades 1, 2, 3, 4, 5 and 8, as recently
77 reviewed (Corratge-Faillie and Lacombe, 2017;Wang et al., 2018). Hence, for some NPF substrates,
78 transport activity appears relatively confined to distinct subclades with high degree of amino acid
79 identity (e.g. the glucosinolate transporters GTR1-3 (NPF2.9-NPF2.11) with >60% identity and the
80 peptide transporters (NPF8.1-8.3) with > 55% identity - excluding PTR3 (NPF5.2). In contrast, for
81 other substrates such as the 25 putative NPF-GA transporters and the many low-affinity nitrate

82　transporters from *Arabidopsis* (Supplementary Table 1); there is no apparent phylogenetic clustering
83　within distinct subclades. This discrepancy could be due to features other than determinants of GA
84　substrate specificity weighing higher towards defining phylogenetic differentiation. Alternatively, it
85　is conceivable that the current number of putative GA transporters may be overestimated. The
86　ExxE[K/R] motif plays a role in coupling proton and substrate transport in the NPF proteins but
87　otherwise our knowledge on the transport mechanism of NPF members remains limited (Jørgensen et
88　al., 2015). Analysis of the recent crystal structures of *Arabidopsis* NPF6.3 suggested that its
89　enigmatic dual affinity transport mode is controlled by Thr101 phosphorylation-dependent
90　dimerization (Liu and Tsay, 2003) and that nitrate binds to His356 that is only conserved in one out
91　of the ~20 other suggested NPF nitrate transporters (Parker and Newstead, 2014;Sun et al., 2014;He
92　et al., 2017;Wang et al., 2018). The structure of NPF6.3 provides a welcomed basis for inferring
93　structure-function relationships for the NPF proteins but has so far not been used to explain the
94　molecular determinants of substrate specificities of any NPF transporter towards organic molecules.

95　The knowledge gap in our understanding of the relationship between structure and function of NPF
96　transporters complicates the identification NPF transporter substrates based on phylogenetic
97　relationships. Hence, understanding the intricate details of substrate selectivity among plant NPF
98　members will be crucial for predicting and elucidating physiological functions.

99　Here, we aim to increase our understanding of the relationship between structure and function of
100　plant NPF-GA transporters by searching for distinct features among potential substrate-interacting
101　residues within the substrate-binding cavity of GA transporting NPF proteins. In this context, it is
102　paramount to ascertain the *in vitro* data assigning GA transport activity to individual NPF members.
103　To achieve this, we develop and optimize a short-term quantitative GA transport assay in *Xenopus*
104　oocytes that in theory is capable of identifying both GA importers and exporters, and simultaneously
105　detects transport of intermediate-, bioactive- and catabolic GA species. We use the optimized
106　transport assay to identify candidate *Arabidopsis* NPF-GA transporters by characterizing and
107　critically assessing the GA substrate preference map among all *Arabidopsis* NPF members. A
108　surprising result from our study is that some NPF proteins are capable of profoundly altering
109　intracellular pH in *Xenopus* oocytes. In a case study, we show that such alterations may lead to
110　changed accumulation equilibria of membrane permeable phytohormones. In addition, we generate a
111　map of all amino acid residues within the substrate-binding cavity of NPF proteins that may play a
112　role in determining substrate specificity and use the GA substrate preference map to correlate GA
113　transport activity to structural features of NPF proteins. Our findings provide a set of critical
114　considerations that will help in guiding physiological investigations.

115

2　Material and Methods

2.1　Cloning the entire NPF and cRNA generation

118　Coding DNA sequences of the entire *Arabidopsis* NPF were cloned into the *Xenopus* oocyte
119　expression vector, pNB1u as indicated in (Supplementary Table 2) (Nour-Eldin et al., 2006). 17 of
120　the CDS were obtained as uracil-containing non-clonal DNA fragments, codon optimized for
121　*Xenopus* oocyte expression from Thermo Fisher Scientific Geneart wherein a uracil had been placed
122　at either end to facilitate direct insertion into pNB1u via USER cloning (Jørgensen, 2017). Nine of
123　the CDS were amplified via PCR from *Arabidopsis* cDNA. 15 of the CDS were amplified from
124　vectors obtained from Pro. Wolf B. Frommer or Dr. Eilon Shani. Nine of the CDS were amplified
125　from vectors obtained from RIKEN Bioresource Center (BRC) (Seki et al., 1998;Seki et al., 2002).

126   The remaining three CDS had been cloned into pNB1u in a previous study (Nour-Eldin et al., 2012).
127   Primers used for PCR amplification are indicated in (Supplementary Table 2). All PCR amplified
128   fragments had a uracil incorporated at either end via the primers and were cloned into pNB1u via
129   USER cloning as described previously (Nour-Eldin et al., 2006). We used the X7 polymerase
130   (Nørholm, 2010) in the PCR reactions. Linearized DNA templates for RNA synthesis were obtained
131   by PCR amplifying the coding sequences surrounded by *Xenopus* β-Globin 5'- and 3'- UTRs from
132   pNB1u   using   forward   primer   (5'   –
133   AATTAACCCTCACTAAAGGGTTGTAATACGACTCACTATAGGG – 3') and reverse primer (5'
134   – TTTTTTTTTTTTTTTTTTTTTTTTTTTTTTATACTCAAGCTAGCCTCGAG – 3') PCR products
135   were purified using E.Z.N.A Gel extraction kit (Omega Bio-tek) using the manufacturer's
136   instructions. PCR products were *in vitro* transcribed using the mMessage mMachine T7 transcription
137   kit (InVitrogen) using the manufacturer's instructions.

138

2.2   Synthesis of JA-Ile

140   JA-Ile conjugate was chemically synthesized as described in (Kramell et al., 1988).

141

2.3   *Xenopus* oocyte transport assays

143   Defolliculated *Xenopus laevis* oocytes (stage V-VI) were purchased from Ecocyte Biosciences and
144   were injected with 25 ng cRNA in 50.6 nl (500 ng/µl) using a Drummond Nanoject II and incubated
145   for 2-4 days at 16 °C in HEPES-based kulori (90 mM NaCl, 1 mM KCl, 1 mM $MgCl_2$, 1 mM $CaCl_2$,
146   5 mM HEPES pH 7.4) before use. Expressing oocytes were pre-incubated in MES-based kulori (90
147   mM NaCl, 1 mM KCl, 1 mM $MgCl_2$, 1 mM $CaCl_2$, 5 mM MES pH 5) for 4 min, before being
148   transferred to phytohormone-containing MES-based kulori for 60 min. Afterwards, oocytes were
149   washed 3 times in 25 ml HEPES-based kulori followed by one wash in 25 ml deionized water,
150   homogenized in 50 % methanol and stored for >30 min at -20 °C. Following centrifugation (25000 g
151   for 10 min 4 °C), the supernatant was mixed with deionized water to a final methanol concentration
152   of 20 % and filtered through 0.22 µm (MSGVN2250, Merck Millipore) before analytical LC-MS/MS
153   as described below.

154

2.4   pH stabilization

156   Expressing oocytes were injected with 50.6 nl 0.5 M MES 50 mM EGTA adjusted to pH 5.7 with 0.5
157   M TRIS for stabilizing internal oocyte pH to ~6.25 or 0.5 M TRIS 50 mM EGTA adjusted to 7.7
158   with 0.5 M MES for stabilizing internal oocyte pH to ~7.5. Assays were carried out as described
159   above, with the exceptions that sorbitol was included in the MES and the HEPES-based kulori
160   solutions to a final concentration of 50 mM to avoid oocyte swelling, and the timeframe between
161   injection of pH stabilizing buffer to assay was terminated was held to a maximum 30 min.

162

2.5   Metabolite quantification by LC-MS/MS

164 Compounds in the diluted oocyte extracts were directly analyzed by LC-MS/MS. The analysis was
165 performed with modifications from the method described in (Tal et al., 2016). In brief,
166 chromatography was performed on an Advance UHPLC system (Bruker, Bremen, Germany).
167 Separation was achieved on a Kinetex 1.7u XB-C18 column (100 x 2.1 mm, 1.7 μm, 100 Å,
168 Phenomenex, Torrance, CA, USA) with 0.05% v/v formic acid in water and acetonitrile (with 0.05%
169 formic acid, v/v) as mobile phases A and B, respectively. The elution profile for GAs, glucosinolates
170 and glycylsarcosine was: 0-0.5 min, 2% B; 0.5-1.3 min, 2-30% B; 1.3-2.2 min 30-100% B, 2.2-2.8
171 min 100%; 2.8-2.9 min 100-2% B and 2.9-4.0 min 2% B. The elution profile for ABA, jasmonic acid
172 (JA), Ja-Ile and oxo-phytodienoic acid (OPDA) was: 0-0.5 min, 2% B; 0.5-1.2 min, 2-30% B; 1.2-2.0
173 min 30-100% B, 2.0-2.5 min 100%; 2.5-2.6 min 100-2% B and 2.6-4.0 min 2% B. The mobile phase
174 flow rate was 400 μl∗min^{-1} and column temperature was maintained at 40 °C. The liquid
175 chromatography was coupled to an EVOQ Elite triple quadrupole mass spectrometer (Bruker,
176 Bremen, Germany) equipped with an electrospray ion source operated in positive and negative
177 ionization mode. Instrument parameters were optimized by infusion experiments with pure standards.
178 For analysis of GAs, glucosinolates and glycylsarcosine the ion spray voltage was maintained at
179 +4000 V and -4000 V in positive and negative ionization mode, respectively and heated probe
180 temperature was set to 200 °C with probe gas flow at 50 psi. For ABA, JA, JA-Ile and OPDA the ion
181 spray voltage was maintained at -3300 V in negative ionization mode and heated probe temperature
182 was set to 120 °C with probe gas flow at 40 psi. Remaining settings were identical for all analytical
183 methods with cone temperature set to 350 °C and cone gas to 20 psi. Nebulizing gas was set to 60 psi
184 and collision gas to 1.6 mTorr. Nitrogen was used as probe and nebulizing gas and argon as collision
185 gas. Active exhaust was constantly on. Multiple reaction monitoring was used to monitor analyte
186 parent ion → product ion transitions for all analytes: Multiple reaction monitoring transitions and
187 collision energies were optimized by direct infusion experiments. Detailed values for mass transitions
188 can be found in (Supplemental Table 3). Both Q1 and Q3 quadrupoles were maintained at unit
189 resolution. Bruker MS Workstation software (Version 8.2.1, Bruker, Bremen, Germany) was used for
190 data acquisition and processing. Linearity in ionization efficiencies were verified by analyzing
191 dilution series of standard mixtures. Sinigrin glucosinolate was used as internal standard for
192 normalization but not for quantification. Quantification of all compounds was achieved by external
193 standard curves diluted with the same matrix as the actual samples. All GAs were analyzed together
194 in a single method apart from GA12 which suffered from severe ion suppression when combined
195 with the other GAs. Samples with GA12 were therefore analyzed separately and with separate
196 dilution series for quantification. Similarly, other hormones than GAs (ABA, JA, JA-Ile and OPDA)
197 were analyzed in separate analytical runs. Glycylsarcosine and 4-methylthio-3-butenyl were analyzed
198 in a combined analytical run.

199

2.6   pH measurements of oocyte lumen

201 pH-electrodes were pulled from borosilicate glass capillaries (KWIK-FIL TW F120-3 with filament)
202 on a vertical puller (Narishige Scientific Instrument Lab), baked for 120 min at 220 °C and silanized
203 for 60 min with dimethyldichlorosilane (Silanization Solution I, Sigma Aldrich). Electrodes were
204 backfilled with a buffer containing 40 mM KH_2PO_4, 23 mM NaOH and 150 mM NaCl (pH 7.5). The
205 electrode tip was filled with a proton-selective ionophore cocktail (hydrogen ionophore I cocktail A,
206 Sigma-Aldrich) by dipping the tip into the cocktail. Oocytes, as described above, were placed in
207 freshly made HEPES-based ekulori (2 mM $LaCl_3$, 90 mM NaCl, 1 mM KCl, 1 mM $MgCl_2$, 1 mM
208 $CaCl_2$, 5 mM HEPES pH 7.4) for at least 30 min prior to three-electrode voltage clamp experiments.
209 Before each oocyte a pH calibration curve was made for each oocyte using 100 mM KCl pH 5.5, 100
210 mM KCl pH 6.5 and 100 mM KCl pH 7.5. Oocytes were clamped at 0 mV and perfused with

211   HEPES-based ekulori pH 7.4, followed by MES-based ekulori (2 mM LaCl$_3$, 90 mM NaCl, 1 mM
212   KCl, 1 mM MgCl$_2$, 1 mM CaCl$_2$, 5 mM MES pH 5) and internal pH response was measured
213   continuously as a function of external pH change.

214

2.7   Multiple sequence alignment and structure guided identification of cavity lining residues

216   In order to bring the GA transport function into a structural context, NPF protein sequences from the
217   31 plant genomes and two outgroups as performed by (Léran et al., 2014) were retrieved from
218   Phytozome version 9.1(Goodstein et al., 2012) and annotated with their NPF IDs (Léran et al., 2014).
219   Guided by blastp (Altschul et al., 1990), long sequences comprising either multiple NPF modules, or
220   fusions with other proteins, were trimmed to the size of single NPF proteins. Initially, the eight NPF
221   subclades were treated separately, for practical reasons and to facilitate robust multiple sequence
222   alignments produced by MUSCLE (Edgar, 2004). For each group, the *Arabidopsis* NPF6.3 sequence
223   was included as a structural reference (PDB: 4OH3) (Sun et al., 2014). Sequences that due to inserts
224   or gaps were not consistent with an intact Major Facilitator Superfamily (MFS) fold were discarded.
225   In the end, the trimmed multiple sequence alignments for all eight NPF subclades were combined and
226   re-aligned using MAFFT (Katoh and Standley, 2013) followed by manual adjustments. The final
227   alignment comprises 1585 NPF sequences.

228   In order to embrace structural variability in the substrate binding site, the selection of a subset of
229   amino acid positions that defines the substrate-binding site was guided using four crystal structures of
230   bacterial POT family members, including two complexes with the peptidomimetic drug alafosfalin
231   with different binding modes, as well as homology models constructed to represent the outward-
232   facing conformation of the transporters. The four bacterial POT structures (PDB: 4IKZ, 4LEP, 2XUT
233   and 4APS) (Newstead et al., 2011;Solcan et al., 2012;Doki et al., 2013;Guettou et al., 2013), all in
234   inward-facing conformations, were superimposed and surface-exposed residues within 8 Å from the
235   alafosfalin in either of the structures were extracted and included in the subset of amino acids that
236   makes up the binding site residues.

237   Importantly, all known POT structures represent inward-open conformations of the transporter,
238   whereas generally substrate recognition from uptake, will occur when the transporter is in the
239   outward-open orientation. In an attempt to identify residues that line the substrate-binding cavity in
240   the outward-facing conformation, homology models were constructed based on outward-open
241   structures of members of the MFS. The two different outward-open structures of FucP and YajR
242   (PDB: 3O7Q and 3WDO) (Dang et al., 2010;Jiang et al., 2013) were used as templates. Sequence
243   alignments of GkPOT (PDB: 4IKZ) (Doki et al., 2013), FucP and YajR sequences were made with
244   PROMALS3D (Pei et al., 2008) and further refined by hand. Outward-facing homology models of
245   GkPOT were made using MODELLER v9.12 (Sali and Blundell, 1993). Finally, surface-exposed
246   residues within 12 Å from the central cavity (as measured from R36-NH1 and W306-CZ2,
247   respectively) were extracted and included in the binding site residue subset. Our final binding site
248   residue subset, defining the substrate-binding cavity, comprises 51 positions. The sequence logos of
249   GA transporters and non-GA transporters were prepared by the WebLogo program (Crooks et al.,
250   2004).

251

2.8   Principal Component analysis

6

253 The Principal Component Analysis (PCA) was performed with KNIME using the PCA Compute
254 node (Berthold et al., 2008).

255

3   Results

3.1   *Xenopus* oocyte membrane permeability towards GAs at different external pH

258 GAs are weak organic acids with lipophilic properties. Consequently, when heterologous transport
259 assays utilize external media with an acidic pH, membrane permeable GAs will be subject to the so-
260 called ion-trap mechanism (Rubery and Sheldrake, 1973). Whereas import can occur by simple
261 diffusion, export likely necessitates the activity of a transport protein (Kramer, 2006;Binenbaum et
262 al., 2018). Of the more than 130 different GAs existing in nature (MacMillan, 2001) a handful has
263 been tested in various *in vitro* transport assays and shown varying membrane permeation (Saito et al.,
264 2015;David et al., 2016;Kanno et al., 2016;Tal et al., 2016). In particular, products of the C13-
265 hydroxylation pathway appear less membrane permeable than their non C13-hydroxylated
266 counterparts (Binenbaum et al., 2018). To investigate this in more detail, we exposed water injected
267 control oocytes to a 50 µM equimolar mixture of eight different GAs (GA1, GA3, GA4, GA7, GA8,
268 GA9, GA19 and GA24) at three different external pH values (pH 4.7, pH 5.3 and pH 6.0) for 60 min
269 and subsequently quantified internalized GA by LC-MS/MS analysis of oocytes homogenates
270 (Figure 1a). The eight GAs represent intermediate, bioactive and catabolic GA species and
271 characteristically contain a varying number of oxygen atoms (Figure 1b). Four of the GAs (GA4,
272 GA7, GA9 and GA24) appeared to permeate the membrane as they were detected in oocytes at all
273 external pH values whereas the remaining four GAs (GA1, GA3, GA8 and GA19) were not detected
274 in oocytes regardless of the external pH. Increasing the external pH lowered the accumulation of
275 membrane permeable GAs. Based on the quantification, we categorized three of the permeating GAs
276 (GA4, GA7 and GA24) as moderately permeating (oocyte GA concentration ≤ external concentration
277 at pH 5.3 and 6.0, respectively) and one (GA9) as highly permeating (internal concentration 20-80
278 fold over external concentration at pH 6 to 4.7). From this dataset, we draw a simple correlation
279 between number of oxygen atoms and membrane permeability (Figure 1c). Irrespective of oxygen
280 positions on the GA backbone or the functional group in which they participate, GAs with 6 or more
281 oxygens (GA1, GA3, GA8 and GA19), did not permeate the *Xenopus* oocyte membrane at any pH. In
282 comparison, GAs with 5 oxygens (GA4, GA7 and GA24) permeate moderately and GAs with only 4
283 oxygens (GA9) permeate to a high degree. Thus, background accumulation due to diffusion of
284 protonated membrane permeating GAs can - not surprisingly - be minimized by increasing external
285 pH in transport assays. It should be emphasized here that we only investigated membrane
286 permeability toward various GAs in *Xenopus* oocytes and that similar permeability/background
287 uptake cannot necessarily be inferred for other heterologous hosts such as yeast. For example, GA3,
288 which does not permeate oocytes appears to accumulate weakly in yeast (Saito et al., 2015;David et
289 al., 2016;Kanno et al., 2016;Tal et al., 2016).

290

3.2   Determining optimal pH for GA transport assays in *Xenopus* oocytes expressing NPF
         proteins

293 To determine a suitable pH for GA transport assays in *Xenopus* oocytes, we used NPF3.1 as a study
294 case. This transporter imports a wide range of GA species when expressed in *Xenopus* oocytes and
295 assayed at pH 5 (Tal et al., 2016). However, no difference to mock can be seen when exposed to

7

296 highly permeating GAs such as GA9 or GA12. One explanation could be that the strong diffusion of
297 GA9 into oocytes may mask any transport activity (Figure 1a). We have previously shown that
298 transport activity of NPF3.1 is undetectable at pH 7 (Tal et al., 2016). Here, we test the activity of
299 NPF3.1, in a 180 min time-course uptake assay towards 50 μM of the non-permeating GA3 at pH 5
300 and 6 (Figure 2a). At pH 5, NPF3.1-mediated accumulation of GA3 reached equilibrium after
301 approximately 120 min incubation (~1.5 fold x external medium concentrations). At pH 6, NPF3.1-
302 mediated GA3 uptake also reached equilibrium after two hours incubation albeit the equilibrium level
303 was approximately 75 % lower than at pH 5. For comparison, we tested the membrane permeability
304 of GA9 in a 180 min time-course assay in water injected control oocytes (Figure 2b). Accordingly,
305 seeking a compromise between reduced diffusion and reduced transport activity, we retested whether
306 NPF3.1-mediated transport of GA9 into oocytes could be detected at pH 5.5 and pH 6. No difference
307 could be seen to mock oocytes when assayed at pH 5.5 (i.e. both accumulated GA9 to equally high
308 levels). In comparison, when assayed at pH 6, NPF3.1 expressing oocytes accumulate higher
309 amounts of GA9 compared to water injected control oocytes (Figure 2c). Thus, for characterizing
310 NPF protein mediated transport of highly permeating GAs in *Xenopus* oocytes, it can be advisable to
311 adjust external media to pH values >5.5 to reduce diffusion to an extent where the contribution of
312 transport activity is distinguishable. As the transport activity is dramatically reduced at pH 6 (Figure
313 2a) we opted for exploring NPF3.1 transport activity towards our selection of non-permeating GAs at
314 pH 5, moderately permeating GAs at pH 5.5 and highly permeating GAs (including GA12) at pH 6.
315 We detected significantly higher accumulation compared to water injected control oocytes for all
316 non-permeating, moderately permeating and highly permeating GAs at pH 5, pH 5.5 and pH 6,
317 respectively (Supplementary Figure 1). Thus, we established optimized conditions for quantitative
318 GA transport assays capable of detecting NPF3.1-mediated accumulation of eight different GAs
319 including the highly membrane permeating species.

320

3.3 The proton potassium antiport activity portraits an efflux transporter artefact

322 In theory, passive diffusion of moderately permeating GA into oocytes allows screening for
323 exporting transport proteins. For example, if an oocyte expressing a candidate exporter accumulates
324 less GA4 compared to mock oocytes, it could indicate that a portion of the GA4 molecules that have
325 diffused into the transporter expressing oocytes can move out of the oocyte through the transporter.
326 In our preparatory phases we exposed parts of our NPF library to a mixture of phytohormones at
327 external pH 5. The mixture included JA, which highly permeates oocyte membranes at acidic pH.
328 Strikingly, three related transporters, NPF7.1-7.3 all accumulated 75-85% less JA compared to water
329 injected control oocytes (Figure 3a). Our excitement about having identified potential JA exporters
330 was, however, curbed by several factors. Firstly, in an attempt to determine the transporters' substrate
331 preference, we exposed NPF7.3 expressing oocytes to five different phytohormones with lipophilic
332 weak acid properties (GA4, ABA, JA, JA-Ile and OPDA). Despite the diversity in chemical
333 structures, NPF7.3 expressing oocytes accumulated significantly less of all five phytohormones
334 compared to water injected control oocytes (Figure 3b). Thus, either this putative exporter appeared
335 to possess the same enigmatic multi-substrate specificity towards phytohormones as described for
336 other NPF proteins (Kanno et al., 2012;Chiba et al., 2015;Tal et al., 2016) or the reduced
337 accumulation within oocytes was possibly due to indirect effects. In the context of *in vitro* transport
338 assays, the accumulation equilibrium generated by the ion-trap mechanism is expectedly sensitive to
339 small pH changes on either side of the membrane (Rubery and Sheldrake, 1973). Recently, NPF7.3
340 was shown to exhibit a non-electrogenic proton/potassium antiport activity when expressed in
341 oocytes. However, the effect of the imported protons on internal oocyte pH was not investigated (Li

8

342 et al., 2017). This prompted us to measure intracellular pH in oocytes expressing NPF7.3 using a
343 proton-selective electrode in a three-electrode voltage clamp setup. Oocytes were clamped at a
344 membrane potential of 0 mV and perfused with kulori at pH 7.4. This was followed by 400 secs
345 perfusion with ekulori buffer pH 5.0 and then back to pH 7.4 for additional 400 secs, while the
346 intracellular pH was monitored continuously. Compared to water injected control oocytes, NPF7.3
347 expressing oocytes displayed a significant 0.24 pH-units higher cytosolic pH in buffers with pH 7.4.
348 However, within 400 secs intracellular pH markedly dropped by 0.5 pH units when external pH was
349 lowered from 7.4 to 5.0, reaching a cytosolic pH 0.26 units lower than in water injected control
350 oocytes (Figure 3c). During prolonged exposure (60 min) to ekulori buffer pH 5.0 intracellular pH
351 even decreased to a stable pH of approximately 6.3, that completely reversed when re-subjected to
352 pH 7.4 (Supplementary Figure 2). In comparison, oocytes individually expressing a selection of other
353 NPF members; NPF2.5, NPF2.13, NPF3.1, NPF4.1, NPF4.3 and NPF4.6 (Figure 4) did not display a
354 drop in intracellular pH that was significantly different than water injected control oocytes. Next we
355 tested whether a decrease in intracellular pH of this magnitude affects the accumulation of membrane
356 permeating phytohormones. Due to its rapid diffusion into oocytes, we used JA as a representative
357 example of diffusing phytohormones. First, we investigated JA accumulation in water injected
358 control oocytes wherein pH was lowered by concentrated MES/TRIS buffer (pH 5.7) injection
359 resulting in an oocyte intracellular pH of ~6.25 that was stable for approximately 30 min
360 (Supplementary Figure 3). This procedure mimicked the pH lowering effect of NPF7.3 Next we
361 exposed these oocytes to 100 μM JA for 20 min. In comparison, to oocytes that were not injected
362 with the pH-lowering buffer, oocytes with the buffer-controlled intracellular pH of ~6.25
363 accumulated significantly less JA (Figure 3d). In contrast, when we stabilized intracellular pH of
364 NPF7.3 expressing oocytes to ~7.5 via buffer injection, these oocytes accumulated JA to the same
365 extent as in mock oocytes with no buffer injection (Figure 3d). These results strongly suggest that
366 altered accumulation of phytohormones in NPF7.3 expressing oocytes is an indirect effect of the
367 proton influx and concomitant lowering of intracellular pH.

368

369 3.4   A quantitative screen of the *Arabidopsis* NPF proteins

370 To ascertain the *in vitro* based functional annotation of NPF GA transport activity, we used the
371 optimized GA transport conditions to quantitatively screen for GA transport activity towards non-
372 permeating and moderately permeating GAs in oocytes. Therefore, cRNA for translation of all 53
373 *Arabidopsis* NPF members were injected individually into *Xenopus* oocytes and after three days of
374 expression oocytes were exposed for 60 min at pH 5.5 to mixtures of bioactive GAs (50 μM GA1
375 and 100 μM GA4) (Yamaguchi, 2008), a product of catabolism (50 μM GA8) (Yamaguchi, 2008), a
376 biosynthesis intermediate (50 μM GA19) (Yamaguchi, 2008), phloem transported (50 μM GA24)
377 (Regnault et al., 2015) and the seed specific (50 μM GA3) (Derkx et al., 1994). The data is displayed
378 in two figures (Figure 5 and Figure 6). Figure 5 displays transport activities for non-permeating GAs
379 (GA1, GA3, GA8 and GA19), whereas Figure 6 displays transport activities of the moderately
380 permeating GAs (GA4 and GA24). Un-normalized data is included in (Supplementary Figure 4).
381 From subclade NPF4, only NPF4.1 and NPF4.6 transported non-permeating GAs, where NPF4.6
382 accumulated only ~15% of GA compared to NPF4.1 levels. The only other transporters displaying
383 uptake activities of similar magnitude as NPF4.1 were NPF2.5 and NPF3.1. NPF3.1 imported
384 approximately 40 % of NPF4.1 levels. In comparison, NPF1.1, NPF2.3, NPF2.4, NPF2.7, NPF2.12
385 and NPF2.13 imported GAs to approximately 10-15% of NPF4.1 levels. Thus, no significant uptake
386 was detected in oocytes expressing any NPF member from subclades 5-8, indicating that GA
387 transporters cluster within subclades 1-4.

388   Interestingly, our screen indicates different substrate preferences among the identified GA
389   transporters. However, due to a necessity for more rigorous characterization we did not score
390   differences in preference statistically. However, some clear potential preferences can be seen for a
391   few genes. For example, NPF3.1 appears to prefer the biosynthesis intermediate GA19, whereas
392   NPF2.5 shows a strong preference for the bioactive GA1.

393   Transport data on the moderately permeating GAs identifies significant transport activity for more
394   putative GA transporters than uptake on non-permeating GAs. Significant transport is still confined
395   to subclades 1-4 but with more members of subclades 1 and 2 identified as potential GA transporters,
396   namely (NPF1.2, NPF2.1, NPF2.9, and NPF2.11).

397

3.5   Delineating potential substrate binding residues

399   The uptake results presented above (Figure 5 and Figure 6) shows that the apparent GA transport
400   activities are confined to a subset of NPF proteins from subclades 1-4. If we assume that GA-
401   transporting NPF proteins must have residues that confer GA selectivity compared to non-
402   transporting NPF proteins; a pertinent question is whether the identified NPF members share these
403   residues to form identifiable GA specific motifs.

404   The canonical MFS transporter structure consists of two six-helix bundles connected by a long
405   cytosolic loop; the interface between these two bundles contains the residues that interact with the
406   transported substrate and thus define the substrate specificity. The crystal structure of NPF6.3 is an
407   excellent example of an MFS structure (Parker and Newstead, 2014;Sun et al., 2014). During its
408   transport cycle the transporter will alternate between conformations with the substrate-binding site
409   open to the extracellular side, be occluded, or open to the cytoplasm (Jardetzky, 1966;Abramson et
410   al., 2003;Huang et al., 2003). POT family members and NPF members are closely related (Fei et al.,
411   1994;Léran et al., 2014;Jørgensen et al., 2015). Several POT crystal structures have been co-
412   crystallized with a number of different peptides or peptidomimetic drugs (Doki et al., 2013;Guettou
413   et al., 2014;Lyons et al., 2014;Newstead, 2015;2017). All peptides bind at relatively equivalent
414   positions between the two six-helix bundles. To identify potential specificity determining residues of
415   the NPF proteins we utilized POT structures crystallized in complex with the peptidomimetic drug
416   alafosfalin (PDB: 4IKZ and 4LEP) (Doki et al., 2013;Guettou et al., 2013). Surface exposed residues
417   within an 8 Å sphere around alafosfalin were selected; additionally, residues predicted to be surface
418   exposed in an outward-facing conformation, as judged from comparisons with the FucP and YajR
419   structures (PDB: 3O7Q and 3WDO) (Dang et al., 2010;Jiang et al., 2013) were also selected;
420   yielding a total of 51 residues (Figure 7, Supplementary Video 1. From this set of residues, we
421   created sequence logos for the non-membrane permeating GA (GA1, GA3, GA7, GA19)
422   transporting- versus non-GA transporting *Arabidopsis* NPF proteins (GA(+) and GA(-), respectively
423   in Figure 7) in order to highlight any preferred positions (Crooks et al., 2004). Only a few distinct
424   positions were observed; hereunder arginine in position 16, hereafter denoted Arg^{Pos16} (Lys164 of
425   NPF6.3), Ser^{Pos28} (Trp353 of NPF6.3) and Gln^{Pos31} (Leu359 of NPF6.3) (Figure 7).

426   For assessing the physiochemical environment in the substrate binding cavity in NPF transporters the
427   same set of residues were converted to the position-dependent numerical descriptors, z-scales,
428   developed by (Hellberg et al., 1987). The original z-scales descriptors have been derived by a PCA of
429   29 physicochemical variables describing the properties of the 20 natural amino acids, and represent
430   the hydrophilicity (z_1), steric properties (z_2) and polarity of the amino acid (z_3). The z-scales have
431   successfully been used in several proteochemometric studies, for instance to model HIV protease

432 resistance or to alignment-independently classify G-coupled receptors and more (Lapinsh et al.,
433 2002;van Westen et al., 2013;Cortés-Ciriano et al., 2015). The 51 sequences times 51 residues matrix
434 was converted to a 51 sequences times 153 z-scales matrix, which was subjected to a PCA.

435 The PCA only shows four major clusters indicating shared physicochemical properties in the
436 substrate binding cavity in genes across phylogenetic subclades. Three of the clusters are clearly
437 defined whereas the fourth is larger and more diffuse. Cluster I, contains six NPF2 subclade proteins
438 that include four GA(+) transporters and two GA(-) transporters. Cluster II contains eleven NPF
439 proteins, four GA(+) and seven GA(-) transporters, from the NPF1, NPF2 and NPF3 subclades.
440 Cluster III, contains solely GA(-) transporters from the NPF5 subclade. Finally, cluster IV contains
441 the remaining NPF proteins including the two GA(+) transporters, NPF4.1 and NPF4.6 (Figure 8).
442 Glucosinolate transporting NPF proteins (NPF2.9-2.13 and NPF3.1) (Nour-Eldin et al.,
443 2012;Jørgensen et al., 2017) and peptide transporting NPF proteins (NPF5.2 and NPF8.1-NPF8.3)
444 (Supplementary Figure 5) (Frommer et al., 1994;Dietrich et al., 2004;Hammes et al., 2010) group in
445 two tight groups in distinct clusters in the PCA plot (Figure 8), and both clusters contain additional
446 genes (cluster II and IV, respectively). Similar to GA(+) transporters, nitrate transporters are
447 scattered in more clusters (Supplementary Figure 6).

448 Cluster I is composed exclusively of genes belonging to the NAXT subclade whose members all lack
449 the ExxE[K/R] motif, i.e. the negatively charged Glu^{Pos1} (Residue 41 of NPF6.3), Glu^{Pos2} (Residue 44
450 of NPF6.3) and the positively charged Arg/Lys^{Pos3} (Residue 45 of NPF6.3). This motif is otherwise
451 conserved in the rest of the family except in the NPF7 clade (Segonzac et al., 2007;Jørgensen et al.,
452 2015). To exclude bias by the presence/absence of the ExxE[K/R] motif, the entire PCA was repeated
453 for only 48 residues (i.e. omitting positions 1-3). The 48 residue PCA yielded four clusters containing
454 the same genes and a similar clustering as the PCA on the original 51 residues (Supplementary
455 Figure 7). Thus, cluster I is not defined based on the absence of the ExxE[K/R] motif.

456 In order to identify characteristic properties for each of the four clusters, we created sequence logos
457 for the individual clusters (Figure 9). Besides uniquely lacking the ExxE[K/R] motif, cluster I is the
458 only cluster that includes Ala^{Pos18} (Ser168 of NPF6.3), Asn^{Pos43} (Gln483 of NPF6.3), Thr^{Pos46}
459 (Leu503 of NPF6.3), Ser^{Pos47} (Leu504 of NPF6.3) and Phe^{Pos50} (Phe511 of NPF6.3) (Figure 9, red
460 arrows; Figure 10, green residues). In comparison, only one residue is unique to cluster II, namely
461 Asn^{Pos12} (Residue 82 of NPF6.3) (Figure 9, blue arrow; Figure 10, blue residue). It is interesting to
462 compare the differences between cluster I/II versus cluster III/IV, since the majority of the GA
463 transporters are found in cluster I and II. The sequence logos indicate residues that are uniquely
464 shared between cluster I and II. For example, position 16 (Residue 164 in NPF6.3), is conserved as
465 an Arg in cluster I and II and Lys in cluster III and IV. In addition, Gln^{Pos31} (Residue 359 of NPF6.3),
466 Leu^{Pos37} (Residue 469 of NPF6.3) and Ala^{Pos40} (Residue 477 of NPF6.3) are characteristic for cluster
467 I/II compared to cluster III/IV (Figure 9, black arrows; Figure 10, yellow residues).

468

469 **4   Discussion**

470 Perhaps one of the most intriguing features of the NPF phytohormone transporters is the apparent
471 multi-specificity towards phytohormones and other metabolites with distinct chemical structure
472 (Corratge-Faillie and Lacombe, 2017;Wang et al., 2018). This phenomenon has previously
473 prompted speculations in the NPF, providing a basis for the integration of environmental and
474 physiological information linked to the relative availability of the different nutrients (Corratge-

475   Faillie and Lacombe, 2017). However, to delve into this interesting notion of multi-substrate
476   specificity it becomes pertinent to discuss how to distinguish between "real" and "non-"
477   substrates for NPF transporters. In this context, our data provide some novel points for
478   discussion.

479   Firstly, there appears to be indirect ways that NPF transporters can alter the distribution pattern of
480   membrane permeating substrates with acid/base properties across membranes. For example, our
481   characterization of NPF7.3 provides an alternative explanation to what we first perceived as multi-
482   specificity towards different phytohormones. As NPF7.3 causes a profound reduction in internal
483   oocyte pH when external pH is reduced from 7.4 to 5 (Figure 3c), the strength of the ion-trap
484   mechanism is altered, and this affects the diffusion-based accumulation pattern of lipophilic
485   phytohormones across the membrane regardless of their chemical structure. In this context, it is
486   concerning that current *in vitro* data points to multi-substrate specificity for several NPF
487   phytohormone importers (Supplementary Table 1). It remains to be investigated whether expression
488   of NPF members in heterologous systems can cause increased internal pH that would lead to an
489   increased ion-trap strength and thereby indirect uptake of many structurally unrelated membrane-
490   permeating phytohormones. This could, for example, happen by the outward movement of protons or
491   potentially by transport of buffer molecules through the transporters. Interestingly, *Streptococcus*
492   *thermophilus* PepT1, a POT homolog of NPF transporters was recently co-crystallized together with
493   the buffering reagent HEPES – binding within the cavity (Martinez Molledo et al., 2018). The efflux
494   of protons has not yet been reported for any NPF protein nor has transport of HEPES to the best of
495   our knowledge been investigated. We measured pH in oocytes expressing six different NPF proteins
496   with GA import activity and could not detect altered pH in any of them (Figure 4). However, we
497   cannot exclude that discrete and transient pH alterations may have eluded detection. In conclusion,
498   when considering the results of transport assays involving membrane permeating lipophilic
499   compounds with weak acid/base properties (such as most phytohormones), it is important to consider
500   and exclude indirect factors that may cause changed distribution across the membrane. For example,
501   if using *Xenopus* oocytes it is possible to inject a buffer with enough buffer capacity to maintain
502   internal pH at neutral (Figure 3d).

503   Secondly, NPF2.10 and NPF2.11 (GTR1 and GTR2) transport a wide range of glucosinolates that all
504   share the common glucosinolate core structure but with varying amino acid side chains (Nour-Eldin
505   et al., 2012;Andersen et al., 2013;Jørgensen et al., 2017). Similarly, hPepT1 and hPepT2, two POT
506   transporters involved in dietary peptide uptake in intestines, transport an immense range of
507   peptidomimetics, indicating that a substrate binding cavity accommodating large variations over a
508   common chemical core structure may be a common feature in the NPF (Biegel et al., 2006;Brandsch
509   et al., 2008). Given this apparent plasticity in the substrate-binding cavity, it is conceivable that some
510   NPF members (such as NPF2.10) may accommodate adventitious transport of a wide selection of
511   metabolites (such as GAs) at low levels in heterologous systems. Discerning whether such transport
512   activities represent "real" substrates ultimately, requires deeper insights into the relationship between
513   structure and function of the NPF.

514   Here, we charted the GA substrate preference map of the *Arabidopsis* NPF proteins to elucidate
515   whether it links to distinct structural features within the substrate-binding cavity. Such insights would
516   represent first steps towards understanding the molecular basis of the selectivity of NPF transporters
517   towards organic molecules and lead to an improved ability to predict substrate preference based on
518   sequence information and 3D structure.

519 To date, almost all NPF-GA transporters have been identified using a qualitative and very sensitive
520 substrate dependent growth-based screen in yeast using a two-component GA receptor-based yeast-
521 two-hybrid system (Chiba et al., 2015). In addition, an *in vivo* approach monitored altered
522 accumulation patterns of a fed bioactive fluorescein-conjugated GA3 in *Arabidopsis* transporter
523 mutants. This approach identified NPF3.1 as a *bona fide* GA transporter with a role in
524 accumulating GA in the endodermis (Shani et al., 2013;Tal et al., 2016). Despite the elegance of
525 these approaches, their qualitative nature offers little distinction between transporters with varying
526 transport activity and are, in their current versions, unable to detect transport of non-bioactive GA
527 shown to undergo long distance transport *in planta* (Regnault et al., 2015;Binenbaum et al., 2018).
528 Given its importance for downstream physiological and structure-function investigations, we found a
529 need for critically re-assessing the *in vitro* data for GA substrate specificity among NPF transporters.

530 As a first step, we developed an optimized approach to screen for GA transporters among the
531 *Arabidopsis* NPF members. Unlike previous approaches, the one presented here is quantitative, short-
532 term, not limited to bioactive GAs, and gives preliminary insights into GA substrate specificity
533 (Chiba et al., 2015). This is relevant as only some GAs species have been suggested to be transported
534 long-distances in plants (Regnault et al., 2015). Additionally, compartmentalization has been
535 suggested to play a regulatory role in GA signaling, thus transporters specific for either anabolic or
536 catabolic GA species may be of interest (and can be identified in our screen) (Olszewski et al., 2002).
537 In principle, by screening NPF transporters using a mixture of GAs that include moderately
538 permeating GAs allowed us to screen for both import (increased accumulation) and export (reduced
539 accumulation of permeating GAs) activity. However due to the potential ambiguity associated with
540 interpreting accumulation of diffusing GA (described above), we focus on reporting and analyzing
541 import activity only of non-diffusing GAs. In summary, our screen identified ten *bona fide*
542 *Arabidopsis* NPF GA transporters belonging to subclades 1-4 that transported non-diffusing GAs in
543 oocytes (Figure 5). In parallel, it is equally important to consider which genes our screen did not
544 identify as GA transporters. In contrast to previous *in vitro* data, no members from subclades 5-8
545 were identified in our screen (Chiba et al., 2015). Notably, NPF1.3 appears to lack the large loop
546 between TM6 and TM7 whereas NPF2.2 lacks a large region equal to parts of TM10 and TM11 of
547 NPF6.3, thus it is likely that these two transporters are non-functional (data not shown). In support of
548 the remaining negative uptake data not being false negatives e.g. due to lack of expression we note
549 that 15 of these 39 transporters have previously been expressed functionally in *Xenopus* oocytes;
550 NPF2.8, NPF2.10, NPF2.14, NPF5.5, NPF5.10, NPF5.11, NPF5.12, NPF5.16, NPF6.2, NPF6.3,
551 NPF7.2, NPF7.3 NPF8.1, NPF8.2 and NPF8.3 (Tsay et al., 1993;Chiang et al., 2004;Chiu et al.,
552 2004;Dietrich et al., 2004;Komarova et al., 2008;Li et al., 2010;Nour-Eldin et al., 2012;Léran et al.,
553 2015;He et al., 2017;Jørgensen et al., 2017;Li et al., 2017). In conclusion, the quantitative short-term
554 uptake screen presented here significantly reduces the number of potential *Arabidopsis* GA
555 transporters from 25 to 10 and confines them to NPF subclades 1-4.

556 As a second step, we investigated whether molecular determinants of GA substrate specificity could
557 be found among the transporter cavity exposed residues around the substrate binding sites. To
558 identify these residues, we generated a map of all cavity exposed amino acids within an 8 Å sphere to
559 the substrate binding site in all three conformations (outward open, occluded, inward open). This
560 identified 51 positions in the plant NPF structures that we suggest as a general foundation for
561 structure-function elucidation.

562 PCA analysis of physicochemical properties of the 51 residue subset and corresponding sequence
563 logos did not reveal a clear set of features in the substrate-binding cavity that associated directly with
564 all GA transporting NPFs. However, from our analyses a few residues did emerge that associated

565 with a large portion of GA transporters. Namely, Arg^{Pos16}, $Gln^{Pos31,}$ Leu^{Pos37} and Ala^{Pos40} are either
566 conserved differently in cluster I and cluster II in the PCA analysis of physicochemical properties
567 compared to clusters III and IV or appear as distinct features in the family wide sequence logo
568 analysis. As cluster I and II contains the majority of GA transporters it is possible that some of these
569 residues are important for GA recognition. Incidentally, an investigation of YePepT from *Yersinia*
570 *enterocolitica* identified Lys314 as a determinant of specificity towards negatively charged
571 dipeptides (Boggavarapu et al., 2015). Lys314 of YePepT corresponds to position 31 (Leu359 of
572 NPF6.3) in our alignment, which is highly and uniquely conserved as Gln^{Pos31} among the GA
573 transporting NPF members of cluster I and II. Lastly, position 40 (Ala477 of NPF6.3), conserved as
574 an Ala in cluster I and II, is located adjacent to a Glu which is highly conserved in all POTs where it
575 plays a role in binding the N-terminus of peptides (Meredith et al., 2000;Jensen et al., 2012;Solcan et
576 al., 2012). However, in summary as GA transporters NPF4.1 and NPF4.6 are located in cluster IV
577 and that other specificities are known for members of clusters I and II, our analyses indicate that GA
578 may be recognized differently by different NPF GA transporters.

579 It is intriguing that many of the *Arabidopsis* NPF proteins are able to transport nitrate, without any
580 apparent binding site features substantiating these observations; nitrate is a small molecule and to
581 some extent it might be comprehensible that it would be able to trigger the transport mechanism. Our
582 assay results support previous observations and show that GA, a molecule much larger than nitrate, is
583 essentially able to behave in the same way as nitrate and trigger transport mechanism without having
584 any specific conserved binding site (Figure 8, Supplementary Figure 6). Human PepT1 and related
585 bacterial transporters have been found to be highly promiscuous, nonetheless most if not all of these
586 substrates contain structural remnants of peptides such as an N- or C-terminus, or a peptide bond.
587 These groups presumably help anchoring the molecule in the substrate binding site for long enough
588 to trigger transport. To our knowledge most NPF substrates known to date, as summarized in
589 (Corratge-Faillie and Lacombe, 2017;Wang et al., 2018), contain a chemical group that can exhibit a
590 negative charge but not a positive charge; it is conceivable that this negative charge anchors these
591 substrates to a positively charged group in the binding site. Position 16 contains a conserved positive
592 charge (Figure 7 and Figure 9) and has been shown to interact with the C-terminus of peptides
593 (Jensen et al., 2014). Perhaps the negative charge of NPF substrates, including that of GAs, is what
594 evolution has kept from the chemical properties of the peptides to ensure coupling the
595 electrochemical proton gradient.

596 Lastly, it should be emphasized that functional annotations are of course very sensitive to false
597 positive results. Despite our considerations of technical artifacts, it is still possible that our list of
598 positive GA transporters is over-estimated. As exemplified by the GTRs which transport nitrate
599 poorly and glucosinolates with high affinity (Wang and Tsay, 2011;Nour-Eldin et al., 2012;Jørgensen
600 et al., 2017), we cannot exclude that a better substrate awaits to be identified for a number of the
601 transporters in our list.

602 5   Abbreviations

603 Abscisic acid (ABA), Gibberellic acid (GA). Jasmonic acid (JA), Jasmonoyl-isoleucine (JA-Ile),
604 Major Facilitator Superfamily (MFS), Nitrate transporter 1/Peptide transporter family (NPF), Oxo-
605 phytodienoic acid (OPDA), Principal Component Analysis (PCA), Proton-coupled Oligopeptide
606 Transporter (POT)

607 6   Author contribution

14

608 NW optimized GA assays, performed the screen, participated in pH measurements, analyzed LC-
609 MS/MS data contributed to the study design and wrote the paper based on a draft. MJ did the initial
610 GA experiments including 4-Methylthio-3-butenyl and glycylsarcosine screen and contributed to pH
611 measurements in *Xenopus* oocytes, NPF7.3 characterization, data analysis and the study design. HE
612 made the multiple sequence alignment and defined the binding site residues. SL characterized
613 NPF7.3 mediated phytohormone transport supported by ZB. TM participated in cytosolic pH
614 measurements in *Xenopus* oocytes and data analysis. CC performed the LC-MS/MS analysis. MM
615 synthesized the JA-Ile. DG participated in defining the NPF7.3 effect on the ion-trap mechanism. FJ
616 performed PCA and clustering analysis. OM and HN advised and contributed to the study design.
617 HN wrote the paper based on a draft. All authors discussed the results and commented on the
618 manuscript.
619

620 **7   Funding**

625 **8   Acknowledgements**

628

629 **9   Conflict of interest**

630 The authors declare no conflict of interest.

631

632 **10   Figures**

633
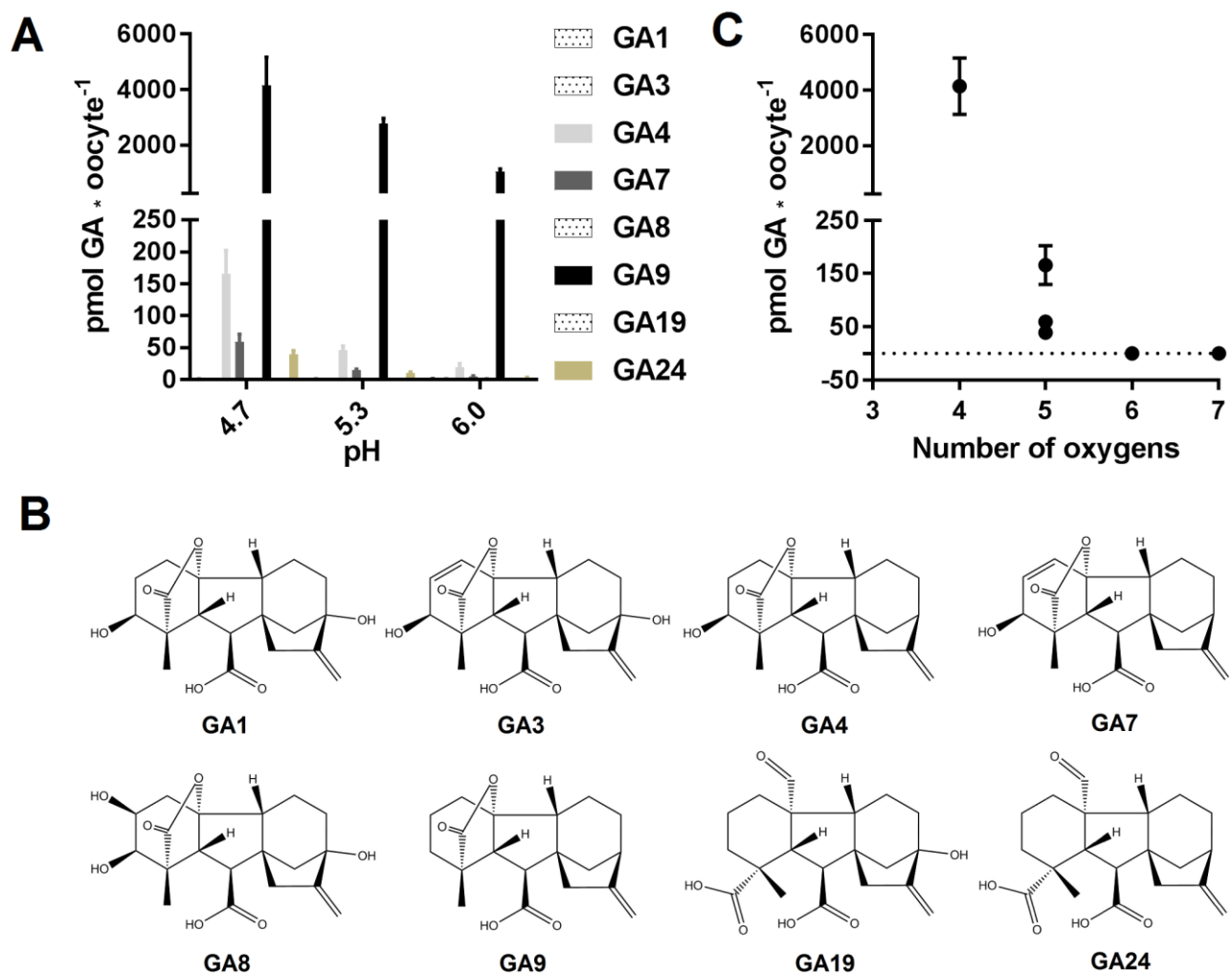
Figure 1. GA membrane permeability is a function of pH and oxygen content. (**A**). Mock expressing oocytes (n = 7-9) were exposed to a mix of 50 μM GA1, 50 μM GA3, 50 μM GA4, 50 μM GA7, 50 μM GA8, 50 μM GA9, 50 μM GA19, and 50 μM GA24 in pH 4.7, 5.3 and 6.0 for 60 min and GA content was quantified by LC-MS/MS. (**B**). Chemical structures of the tested GAs. (**C**). GA content of mock injected oocytes at pH 4.7 as a function of GA oxygen content.
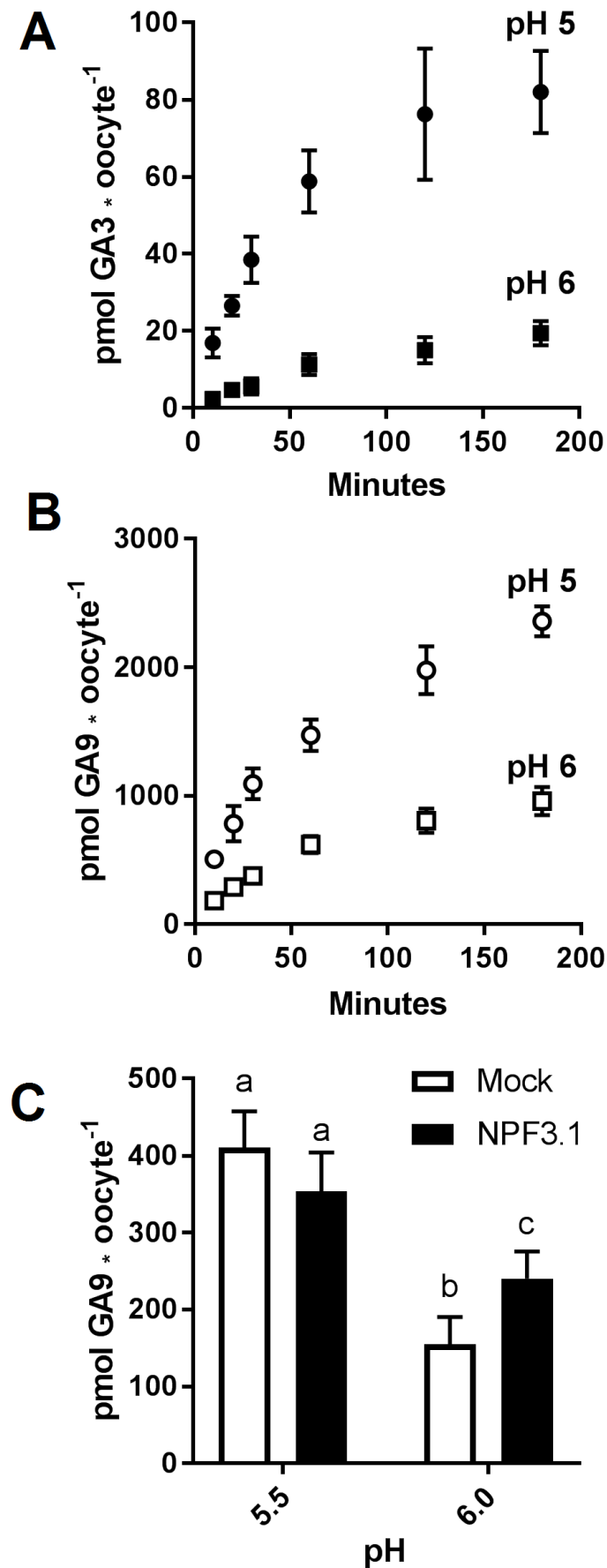
639

640 **Figure 2.** Assessment of GA permeability and NPF transporter function. (**A**). Time course of NPF3.1
641 mediate GA3 transport over 180 min. NPF3.1 expressing oocytes were exposed to 50 µM membrane
642 non-permeable GA3 in kulori pH 5 or 6. At each time point, oocytes (n = 6) were taken out for
643 analysis. (**B**). Time course of GA9 membrane penetration over 180 min. Mock expressing oocytes
644 were exposed to 50 µM GA9 in kulori pH 5 or 6. At each time point, oocytes (n = 6) were taken out
645 for analysis. (**C**). NPF3.1 mediated GA9 transport at pH 5.5 and 6. Oocytes (n = 6) were exposed to
646 50 µM GA9 in kulori (materials and methods) pH 5.5 or 6 for 60 min. Oocyte GA content was
647 analyzed using LC-MS/MS. Statistical assessment was performed with Holm Sidak two-way
648 ANOVA p = 0.01.

	pH$_{ext}$	
	pH 7.4	pH 5.0
NPF7.3	7.56 ± 0.1	7.04 ± 0.14
Mock	7.32 ± 0.03	7.30 ± 0.02

649

18
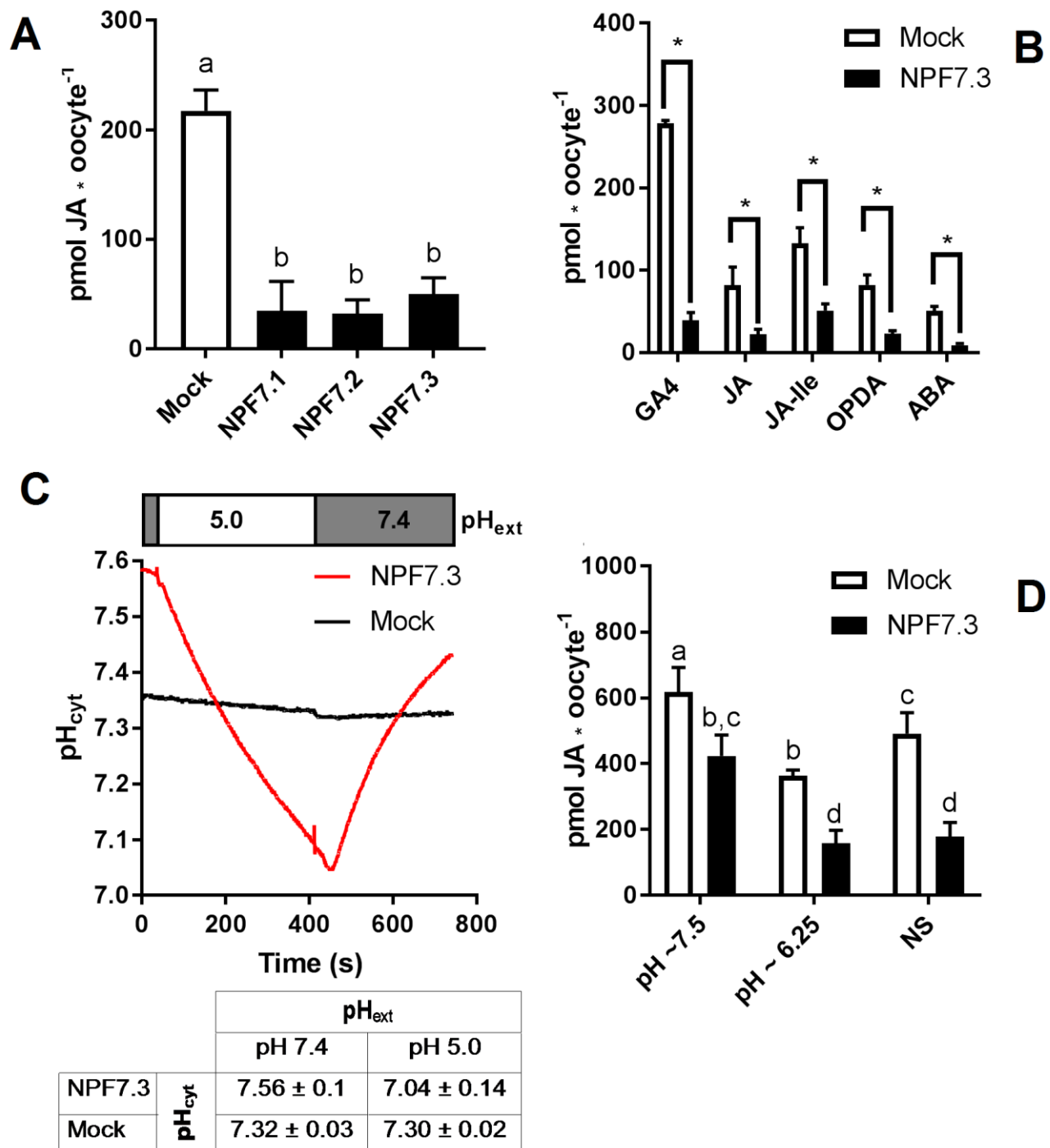
650 **Figure 3**. The proton potassium antiport function of NPF7.3 influences the ion-trap mechanism of
651 membrane permeable weak acids. (**A**). Oocytes were exposed to 100 μM JA in kulori pH 5 for 60
652 min and analyzed in 3 technical replicates of 5 oocytes. Statistical assessment was performed with
653 Holm Sidak one-way ANOVA p = 0.01. (**B**). Lower accumulation of membrane permeable
654 phytohormones in NPF7.3 expressing oocytes compared to mock. Oocytes were exposed to 100 μM
655 phytohormone in kulori pH 5 for 60 min (JA, JA-Ile, OPDA, ABA) or 90 min (GA4) and analyzed in
656 3-4 technical reps of 4-5 oocytes. Statistical assessment was performed with two-tailed t-tests p =
657 0.05 (**C**). Upper panel: Internal oocyte pH measured using three-electrode voltage-clamp of mock vs
658 NPF7.3 expressing oocytes. Starting in ekulori pH 7.4, the external buffer was changed to ekulori pH
659 5.0 for 400 secs followed by ekulori pH 7.4 for another 400 sec. pH was measured continuously at a
660 membrane potential of 0 mV. Representative measurements are shown. Lower panel: Mean values of
661 cytosolic pH in mock or NPF7.3 expressing oocytes in standard ekulori buffer pH 7.4 or 400 secs
662 after incubation in ekulori pH 5.0 (n ≥ 3, mean ± SD). (**D**). JA content at defined cytosolic pH.
663 Oocytes injected with 0.5 M TRIS 50 mM EGTA adjusted to pH 7.7 with 0.5 M MES (pH stabilized
664 at ~7.5), 0.5 M MES 50 mM EGTA adjusted to 5.7 with 0.5 M TRIS (pH stabilized at ~6.25) or
665 water (not stabilized: NS) was exposed to 100 μM JA in kulori pH 5 for 20 min and analyzed in 2 x 3
666 technical reps of 4-5 oocytes. Oocyte phytohormone content was analyzed using LC-MS/MS.
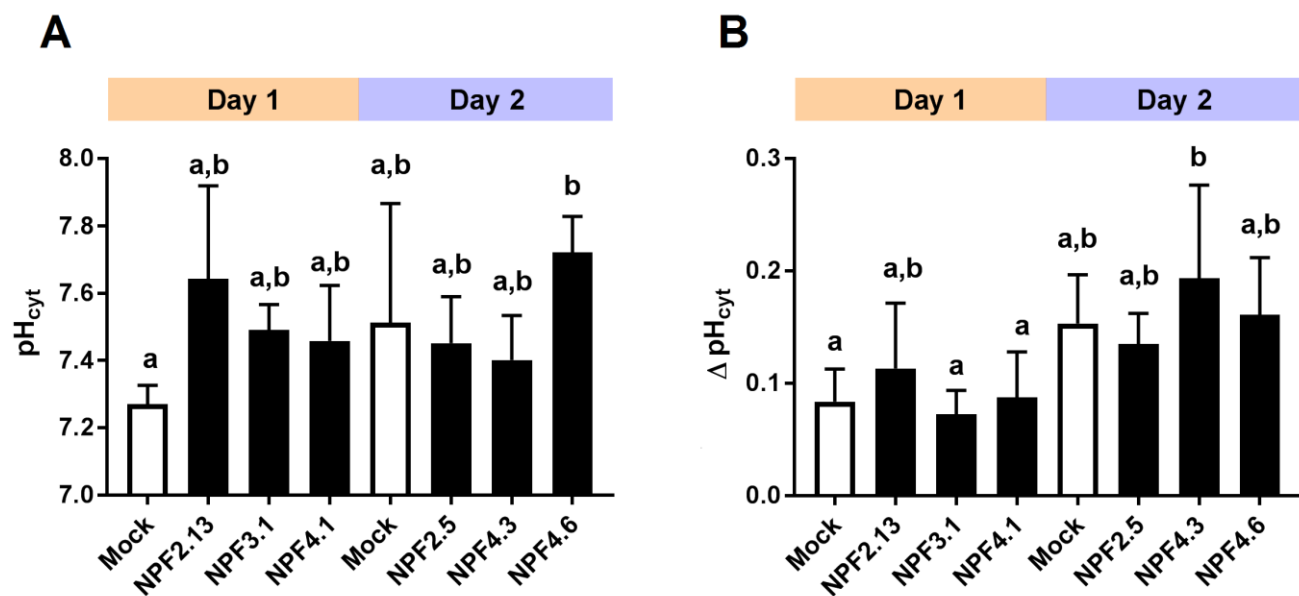667 Statistical assessment was performed with Holm Sidak two-way ANOVA p = 0.01.

668

669 **Figure 4.** Transporter expression and oocyte maturity influence internal oocyte pH. Internal oocyte
670 pH measured using three-electrode voltage-clamp of mock versus expressing oocytes. (**A**). after 30
671 min resting in ekulori pH 7.4 and additional 5 min clamped at 0 mV with pH 7.4 ekulori perfusion.
672 (**B**). Change in internal pH after additional 5 min perfusion with pH 5 ekulori. Statistical assessment

19

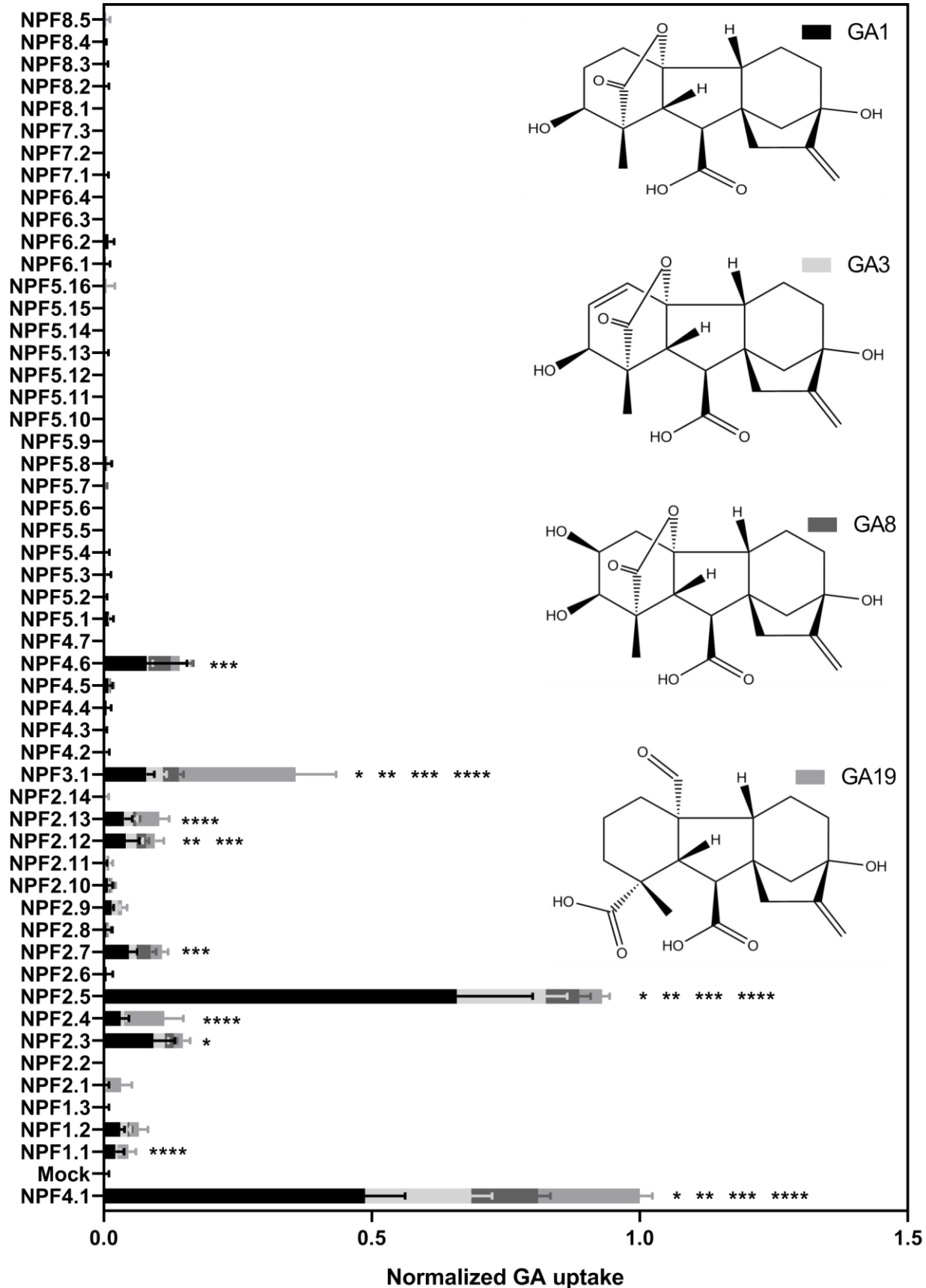673   was performed with Holm Sidak two-way ANOVA p = 0.05.

674

675 **Figure 5.** Quantitative screen of the NPFs for GA transport of not membrane non-permeable GAs.
676 Due to logistic considerations, the 53 NPF members were screened in two portions on the same day
677 and normalized to the transport of NPF4.1 of membrane non-permeable GAs. NPF4.1 was chosen for
678 normalization as it is a well characterized GA transporter (Kanno et al., 2012;Saito et al., 2015;Tal et
679 al., 2016). For each transporter the proportion of each GA imported into oocytes is given in
680 proportion to total imported amount of GAs. Statistical significant transport (Holm Sidak one-way
681 ANOVA p = 0.05) is indicated with one asterisk for GA1, two asterisks for GA3, three asterisks for
682 GA8 and four asterisks for GA19.Two assays of 28 and 29 genes, respectively, were performed on
683 same day on the same oocyte batch. Both assays included NPF3.1, NPF4.1 and Mock in order to
684 normalize. Oocytes (n = 5-6) were exposed to a mix of 50 µM GA1, 50 µM GA3, 100 µM GA4, 50
685 µM GA8, 50 µM GA19 and 50 µM GA24 in pH kulori 5.5 (Materials and Methods) for 60 min.
686 Oocyte GA content was analyzed using LC-MS/MS.
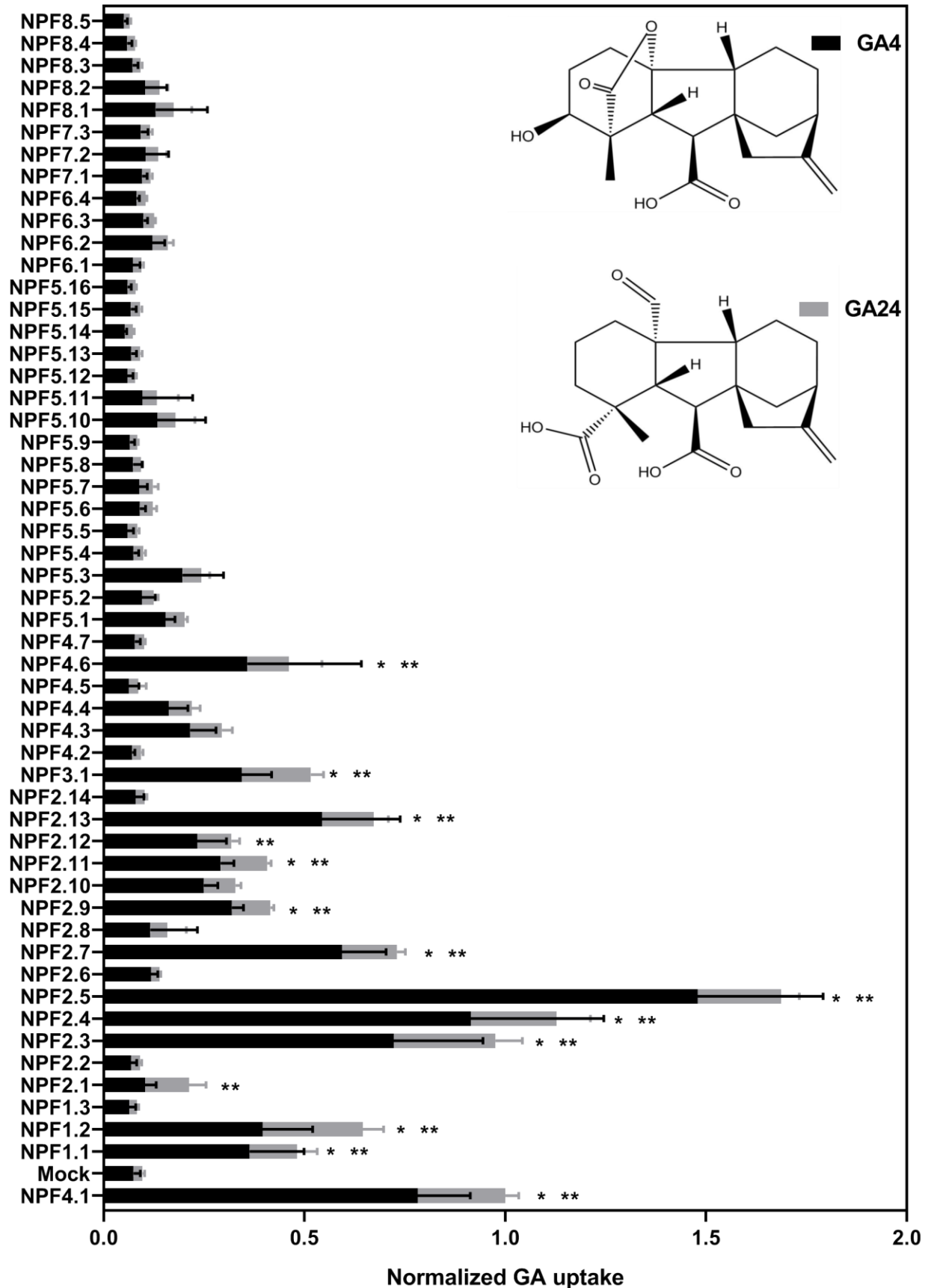
687

23

688   **Figure 6**. Quantitative screen of the NPF proteins for GA transport of membrane permeable GAs.
689   Due to logistic considerations, the 53 NPF members were screened in two portions on the same day
690   and normalized to the transport of NPF4.1 of membrane permeable GAs. NPF4.1 was chosen for
691   normalization as it is a well characterized GA transporter (Kanno et al., 2012;Saito et al., 2015;Tal et
692   al., 2016). For each transporter the proportion of each GA imported into oocytes is given in
693   proportion to total imported amount of GAs. Statistical significant transport (Holm Sidak one-way
694   ANOVA p = 0.05) is indicated with one asterisk for GA4 and two asterisks for GA24. Two assays of
695   28 and 29 genes, respectively, were performed on same day on the same oocyte batch. Both assays
696   included NPF3.1, NPF4.1 and Mock in order to normalize. Oocytes (n = 5-6) were exposed to a mix
697   of 50 µM GA1, 50 µM GA3, 100 µM GA4, 50 µM GA8, 50 µM GA19 and 50 µM GA24 in pH
698   kulori 5.5 (Materials and Methods) for 60 min. Oocyte GA content was analyzed using LC-MS/MS.
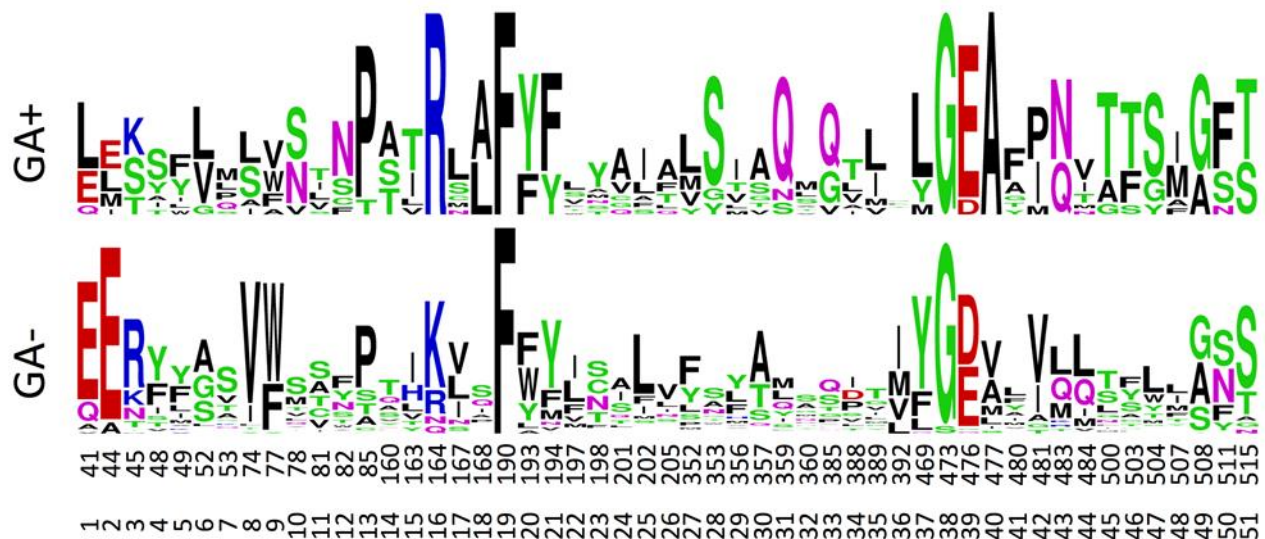

699

700   **Figure 7**. Sequence logos for the GA transporting (GA+) versus GA non-transporting (GA-) NPF
701   proteins. Numbers correspond to the amino acid position of *Arabidopsis* thaliana NPF6.3 and the
702   relative position of the binding site residues. The figure was made in the WebLogo program (Crooks
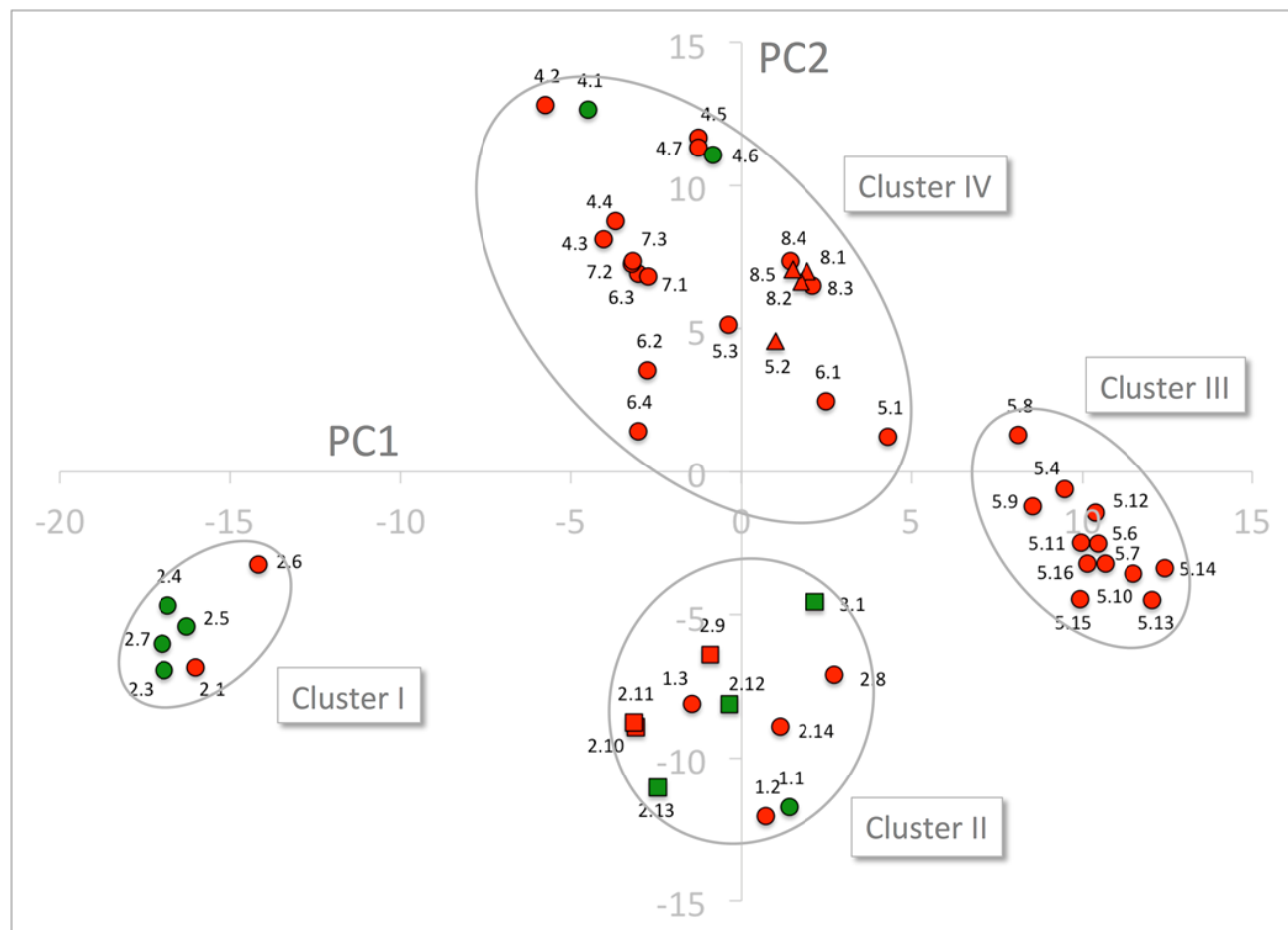703   et al., 2004).

24

704

Figure 8. PCA of the 51 NPF sequences expressed by z-scales. GA transporting transporters are shown as green dots and squares and GA non-transporting transporters as red dots, triangles and squares. Glucosinolate transporting genes and peptide transporting genes are shown as squares and triangles, respectively. The four clusters are marked by ellipses. PC1 and PC2 refer to the first and second principal components, respectively.
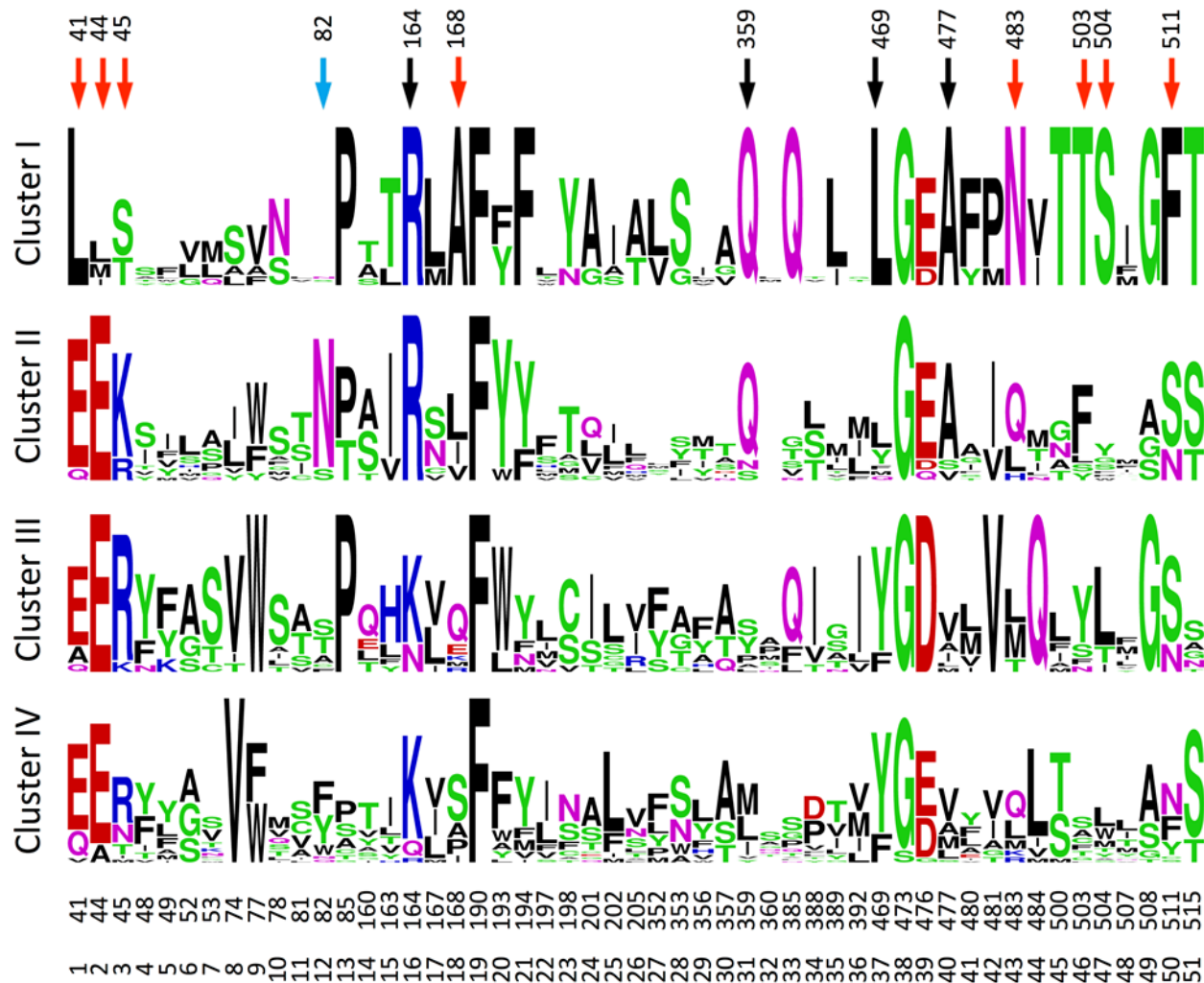
25

Figure 9. Sequence logos for the transporters in the four clusters. The figure was made in the WebLogo program (Crooks et al., 2004). Red, blue and black arrows mark positions unique for cluster I, cluster II and for cluster I and II, respectively.
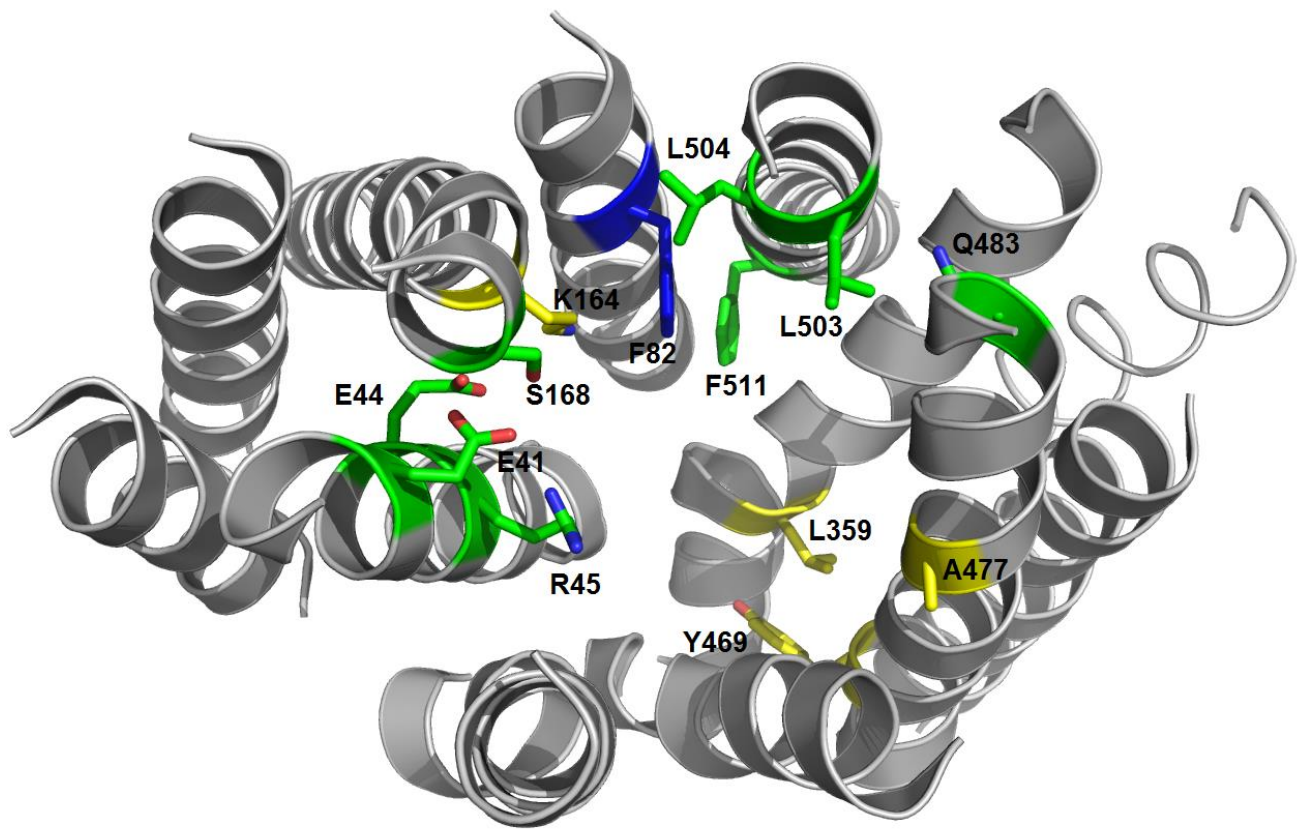
Figure 10. 3D structure of the NPF6.3 (PDB: 4OH3 (Sun et al., 2014)). Residues unique for cluster I are shown as green sticks, the residue unique for cluster II is shown as a blue stick and residues unique for cluster I and II are shown as yellow sticks.

11   References

Abramson, J., Smirnova, I., Kasho, V., Verner, G., Kaback, H.R., and Iwata, S. (2003). Structure and mechanism of the lactose permease of Escherichia coli. *Science* 301**,** 610-615.

Aduri, N.G., Prabhala, B.K., Ernst, H.A., Jørgensen, F.S., Olsen, L., and Mirza, O. (2015). Salt Bridge Swapping in the EXXERFXYY Motif of Proton-coupled Oligopeptide Transporters. *J Biol Chem* 290**,** 29931-29940.

Altschul, S.F., Gish, W., Miller, W., Myers, E.W., and Lipman, D.J. (1990). Basic local alignment search tool. *J Mol Biol* 215**,** 403-410.

Andersen, T.G., Nour-Eldin, H.H., Fuller, V.L., Olsen, C.E., Burow, M., and Halkier, B.A. (2013). Integration of biosynthesis and long-distance transport establish organ-specific glucosinolate profiles in vegetative Arabidopsis. *Plant Cell* 25**,** 3133-3145.

Berthold, M.R., Cebron, N., Dill, F., Gabriel, T.R., Kötter, T., Meinl, T., Ohl, P., Sieb, C., Thiel, K., and Wiswedel, B. (Year). "KNIME: The Konstanz Information Miner": Springer Berlin Heidelberg), 319-326.

733 Biegel, A., Knutter, I., Hartrodt, B., Gebauer, S., Theis, S., Luckner, P., Kottra, G., Rastetter, M.,
734   Zebisch, K., Thondorf, I., Daniel, H., Neubert, K., and Brandsch, M. (2006). The renal type
735   H+/peptide symporter PEPT2: structure-affinity relationships. *Amino Acids* 31**,** 137-156.

736 Binenbaum, J., Weinstain, R., and Shani, E. (2018). Gibberellin Localization and Transport in Plants.
737   *Trends Plant Sci*.

738 Boggavarapu, R., Jeckelmann, J.M., Harder, D., Ucurum, Z., and Fotiadis, D. (2015). Role of
739   electrostatic interactions for ligand recognition and specificity of peptide transporters. *BMC*
740   *Biol* 13**,** 58.

741 Brandsch, M., Knutter, I., and Bosse-Doenecke, E. (2008). Pharmaceutical and pharmacological
742   importance of peptide transporters. *J Pharm Pharmacol* 60**,** 543-585.

743 Chiang, C.S., Stacey, G., and Tsay, Y.F. (2004). Mechanisms and functional properties of two
744   peptide transporters, AtPTR2 and fPTR2. *J Biol Chem* 279**,** 30150-30157.

745 Chiba, Y., Shimizu, T., Miyakawa, S., Kanno, Y., Koshiba, T., Kamiya, Y., and Seo, M. (2015).
746   Identification of Arabidopsis thaliana NRT1/PTR FAMILY (NPF) proteins capable of
747   transporting plant hormones. *J Plant Res* 128**,** 679-686.

748 Chiu, C.C., Lin, C.S., Hsia, A.P., Su, R.C., Lin, H.L., and Tsay, Y.F. (2004). Mutation of a nitrate
749   transporter, AtNRT1:4, results in a reduced petiole nitrate content and altered leaf
750   development. *Plant Cell Physiol* 45**,** 1139-1148.

751 Corratge-Faillie, C., and Lacombe, B. (2017). Substrate (un)specificity of Arabidopsis NRT1/PTR
752   FAMILY (NPF) proteins. *J Exp Bot*.

753 Cortés-Ciriano, I., Ain, Q.U., Subramanian, V., Lenselink, E.B., Méndez-Lucio, O., Ijzerman, A.P.,
754   Wohlfahrt, G., Prusis, P., Malliavin, T.E., Van Westen, G.J.P., and Bender, A. (2015).
755   Polypharmacology modelling using proteochemometrics (PCM): recent methodological
756   developments, applications to target families, and future prospects. *MedChemComm* 6**,** 24-50.

757 Crooks, G.E., Hon, G., Chandonia, J.M., and Brenner, S.E. (2004). WebLogo: a sequence logo
758   generator. *Genome Res* 14**,** 1188-1190.

759 Dang, S., Sun, L., Huang, Y., Lu, F., Liu, Y., Gong, H., Wang, J., and Yan, N. (2010). Structure of a
760   fucose transporter in an outward-open conformation. *Nature* 467**,** 734-738.

761 Daniel, H., and Kottra, G. (2004). The proton oligopeptide cotransporter family SLC15 in physiology
762   and pharmacology. *Pflugers Arch* 447**,** 610-618.

763 David, L.C., Berquin, P., Kanno, Y., Seo, M., Daniel-Vedele, F., and Ferrario-Méry, S. (2016). N
764   availability modulates the role of NPF3.1, a gibberellin transporter, in GA-mediated
765   phenotypes in Arabidopsis. *Planta***,** 1-14.

766 Derkx, M.P.M., Vermeer, E., and Karssen, C.M. (1994). Gibberellins in seeds of Arabidopsis
767   thaliana: biological activities, identification and effects of light and chilling on endogenous
768   levels. *Plant Growth Regulation* 15**,** 223-234.

769 Dietrich, D., Hammes, U., Thor, K., Suter-Grotemeyer, M., Fluckiger, R., Slusarenko, A.J., Ward,
770   J.M., and Rentsch, D. (2004). AtPTR1, a plasma membrane peptide transporter expressed
771   during seed germination and in vascular tissue of Arabidopsis. *Plant J* 40**,** 488-499.

772 Doki, S., Kato, H.E., Solcan, N., Iwaki, M., Koyama, M., Hattori, M., Iwase, N., Tsukazaki, T.,
773   Sugita, Y., Kandori, H., Newstead, S., Ishitani, R., and Nureki, O. (2013). Structural basis for

774   dynamic mechanism of proton-coupled symport by the peptide transporter POT. *Proc Natl*
775   *Acad Sci U S A* 110**,** 11343-11348.

776 Edgar, R.C. (2004). MUSCLE: multiple sequence alignment with high accuracy and high throughput.
777   *Nucleic Acids Res* 32**,** 1792-1797.

778 Fei, Y.-J., Kanai, Y., Nussberger, S., Ganapathy, V., Leibach, F.H., Romero, M.F., Singh, S.K.,
779   Boron, W.F., and Hediger, M.A. (1994). Expression cloning of a mammalian proton-coupled
780   oligopeptide transporter. *Nature* 368**,** 563-566.

781 Frommer, W.B., Hummel, S., and Rentsch, D. (1994). Cloning of an Arabidopsis histidine
782   transporting protein related to nitrate and peptide transporters. *FEBS Letters* 347**,** 185-189.

783 Goodstein, D.M., Shu, S., Howson, R., Neupane, R., Hayes, R.D., Fazo, J., Mitros, T., Dirks, W.,
784   Hellsten, U., Putnam, N., and Rokhsar, D.S. (2012). Phytozome: a comparative platform for
785   green plant genomics. *Nucleic Acids Res* 40**,** D1178-1186.

786 Guettou, F., Quistgaard, E.M., Raba, M., Moberg, P., Low, C., and Nordlund, P. (2014). Selectivity
787   mechanism of a bacterial homolog of the human drug-peptide transporters PepT1 and PepT2.
788   *Nat Struct Mol Biol* 21**,** 728-731.

789 Guettou, F., Quistgaard, E.M., Tresaugues, L., Moberg, P., Jegerschold, C., Zhu, L., Jong, A.J.,
790   Nordlund, P., and Low, C. (2013). Structural insights into substrate recognition in proton-
791   dependent oligopeptide transporters. *EMBO Rep* 14**,** 804-810.

792 Hammes, U.Z., Meier, S., Dietrich, D., Ward, J.M., and Rentsch, D. (2010). Functional properties of
793   the Arabidopsis peptide transporters AtPTR1 and AtPTR5. *J Biol Chem* 285**,** 39710-39717.

794 He, Y.-N., Peng, J.-S., Cai, Y., Liu, D.-F., Guan, Y., Yi, H.-Y., and Gong, J.-M. (2017). Tonoplast-
795   localized nitrate uptake transporters involved in vacuolar nitrate efflux and reallocation in
796   Arabidopsis. *Scientific Reports* 7**,** 6417.

797 Hellberg, S., Sjöström, M., Skagerberg, B., and Wold, S. (1987). Peptide quantitative structure-
798   activity relationships, a multivariate approach. *J Med Chem* 30**,** 1126-1135.

799 Hoad, G.V., and Bowen, M.R. (1968). Evidence for gibberellin-like substances in phloem exudate of
800   higher plants. *Planta* 82**,** 22-32.

801 Huang, Y., Lemieux, M.J., Song, J., Auer, M., and Wang, D.N. (2003). Structure and mechanism of
802   the glycerol-3-phosphate transporter from Escherichia coli. *Science* 301**,** 616-620.

803 Jardetzky, O. (1966). Simple allosteric model for membrane pumps. *Nature* 211**,** 969-970.

804 Jensen, J.M., Aduri, N.G., Prabhala, B.K., Jahnsen, R., Franzyk, H., and Mirza, O. (2014). Critical
805   role of a conserved transmembrane lysine in substrate recognition by the proton-coupled
806   oligopeptide transporter YjdL. *The International Journal of Biochemistry & Cell Biology* 55**,**
807   311-317.

808 Jensen, J.M., Ernst, H., Wang, X., Hald, H., Ditta, A.C., Ismat, F., Rahman, M., and Mirza, O.
809   (2012). Functional investigation of conserved membrane-embedded glutamate residues in the
810   proton-coupled peptide transporter YjdL. *Protein Pept Lett* 19**,** 282-287.

811 Jiang, D., Zhao, Y., Wang, X., Fan, J., Heng, J., Liu, X., Feng, W., Kang, X., Huang, B., Liu, J., and
812   Zhang, X.C. (2013). Structure of the YajR transporter suggests a transport mechanism based
813   on the conserved motif A. *Proc Natl Acad Sci U S A* 110**,** 14664-14669.

814 Jørgensen, M.E., Olsen, C.E., Geiger, D., Mirza, O., Halkier, B.A., and Nour-Eldin, H.H. (2015). A
815   Functional EXXEK Motif is Essential for Proton Coupling and Active Glucosinolate
816   Transport by NPF2.11. *Plant Cell Physiol* 56**,** 2340-2350.

817 Jørgensen, M.E., Wulff, N., Nafisi, M., Xu, D., Wang, C., Lambertz, S. K., Belew, Z. M. And Nour-
818   Eldin, H. H (2017). Design and Direct Assembly of Synthesized Uracil-containing Non-
819   clonal DNA Fragments into Vectors by USERTM Cloning. *Bio-protocol* 7.

820 Jørgensen, M.E., Xu, D., Crocoll, C., Ramírez, D., Motawia, M.S., Olsen, C.E., Nour-Eldin, H.H.,
821   and Halkier, B.A. (2017). Origin and evolution of transporter substrate specificity within the
822   NPF family. *eLife* 6**,** e19466.

823 Kanno, Y., Hanada, A., Chiba, Y., Ichikawa, T., Nakazawa, M., Matsui, M., Koshiba, T., Kamiya,
824   Y., and Seo, M. (2012). Identification of an abscisic acid transporter by functional screening
825   using the receptor complex as a sensor. *Proc Natl Acad Sci U S A* 109**,** 9653-9658.

826 Kanno, Y., Oikawa, T., Chiba, Y., Ishimaru, Y., Shimizu, T., Sano, N., Koshiba, T., Kamiya, Y.,
827   Ueda, M., and Seo, M. (2016). AtSWEET13 and AtSWEET14 regulate gibberellin-mediated
828   physiological processes. *Nature Communications* 7**,** 13245.

829 Katoh, K., and Standley, D.M. (2013). MAFFT multiple sequence alignment software version 7:
830   improvements in performance and usability. *Molecular biology and evolution* 30**,** 772-780.

831 Komarova, N.Y., Thor, K., Gubler, A., Meier, S., Dietrich, D., Weichert, A., Suter Grotemeyer, M.,
832   Tegeder, M., and Rentsch, D. (2008). AtPTR1 and AtPTR5 transport dipeptides in planta.
833   *Plant Physiol* 148**,** 856-869.

834 Kramell, R., Schmidt, J., Schneider, G., Sembdner, G., and Schreiber, K. (1988). Synthesis of n-
835   (jasmonoyl)amino acid conjugates. *Tetrahedron* 44**,** 5791-5807.

836 Kramer, E.M. (2006). How Far Can a Molecule of Weak Acid Travel in the Apoplast or Xylem?
837   *Plant Physiology* 141**,** 1233-1236.

838 Lapinsh, M., Gutcaits, A., Prusis, P., Post, C., Lundstedt, T., and Wikberg, J.E. (2002). Classification
839   of G-protein coupled receptors by alignment-independent extraction of principal chemical
840   properties of primary amino acid sequences. *Protein Sci* 11**,** 795-805.

841 Léran, S., Garg, B., Boursiac, Y., Corratgé-Faillie, C., Brachet, C., Tillard, P., Gojon, A., and
842   Lacombe, B. (2015). AtNPF5.5, a nitrate transporter affecting nitrogen accumulation in
843   Arabidopsis embryo. *Scientific Reports* 5**,** 7962.

844 Léran, S., Varala, K., Boyer, J.-C., Chiurazzi, M., Crawford, N., Daniel-Vedele, F., David, L.,
845   Dickstein, R., Fernandez, E., Forde, B., Gassmann, W., Geiger, D., Gojon, A., Gong, J.-M.,
846   Halkier, B.A., Harris, J.M., Hedrich, R., Limami, A.M., Rentsch, D., Seo, M., Tsay, Y.-F.,
847   Zhang, M., Coruzzi, G., and Lacombe, B. (2014). A unified nomenclature of NITRATE
848   TRANSPORTER 1/PEPTIDE TRANSPORTER family members in plants. *Trends in Plant
849   Science* 19**,** 5-9.

850 Li, H., Yu, M., Du, X.-Q., Wang, Z.-F., Wu, W.-H., Quintero, F.J., Jin, X.-H., Li, H.-D., and Wang,
851   Y. (2017). NRT1.5/NPF7.3 functions as a proton-coupled H+/K+ antiporter for K+ loading
852   into the xylem in Arabidopsis. *The Plant Cell*.

853 Li, J.Y., Fu, Y.L., Pike, S.M., Bao, J., Tian, W., Zhang, Y., Chen, C.Z., Zhang, Y., Li, H.M., Huang,
854   J., Li, L.G., Schroeder, J.I., Gassmann, W., and Gong, J.M. (2010). The Arabidopsis nitrate
855   transporter NRT1.8 functions in nitrate removal from the xylem sap and mediates cadmium
856   tolerance. *Plant Cell* 22**,** 1633-1646.

857   Liu, K.H., and Tsay, Y.F. (2003). Switching between the two action modes of the dual-affinity nitrate
858   transporter CHL1 by phosphorylation. *Embo j* 22**,** 1005-1013.

859   Lyons, J.A., Parker, J.L., Solcan, N., Brinth, A., Li, D., Shah, S.T., Caffrey, M., and Newstead, S.
860   (2014). Structural basis for polyspecificity in the POT family of proton-coupled oligopeptide
861   transporters. *EMBO Rep* 15**,** 886-893.

862   Macmillan, J. (2001). Occurrence of Gibberellins in Vascular Plants, Fungi, and Bacteria. *Journal of*
863   *Plant Growth Regulation* 20**,** 387-442.

864   Martinez Molledo, M., Quistgaard, E.M., Flayhan, A., Pieprzyk, J., and Low, C. (2018).
865   Multispecific Substrate Recognition in a Proton-Dependent Oligopeptide Transporter.
866   *Structure*.

867   Meredith, D., Temple, C.S., Guha, N., Sword, C.J., Boyd, C.A., Collier, I.D., Morgan, K.M., and
868   Bailey, P.D. (2000). Modified amino acids and peptides as substrates for the intestinal peptide
869   transporter PepT1. *Eur J Biochem* 267**,** 3723-3728.

870   Newstead, S. (2015). Molecular insights into proton coupled peptide transport in the PTR family of
871   oligopeptide transporters. *Biochim Biophys Acta* 1850**,** 488-499.

872   Newstead, S. (2017). Recent advances in understanding proton coupled peptide transport via the POT
873   family. *Curr Opin Struct Biol* 45**,** 17-24.

874   Newstead, S., Drew, D., Cameron, A.D., Postis, V.L., Xia, X., Fowler, P.W., Ingram, J.C., Carpenter,
875   E.P., Sansom, M.S., Mcpherson, M.J., Baldwin, S.A., and Iwata, S. (2011). Crystal structure
876   of a prokaryotic homologue of the mammalian oligopeptide-proton symporters, PepT1 and
877   PepT2. *Embo j* 30**,** 417-426.

878   Nour-Eldin, H.H., Andersen, T.G., Burow, M., Madsen, S.R., Jørgensen, M.E., Olsen, C.E., Dreyer,
879   I., Hedrich, R., Geiger, D., and Halkier, B.A. (2012). NRT/PTR transporters are essential for
880   translocation of glucosinolate defence compounds to seeds. *Nature* 488**,** 531-534.

881   Nour-Eldin, H.H., Hansen, B.G., Norholm, M.H., Jensen, J.K., and Halkier, B.A. (2006). Advancing
882   uracil-excision based cloning towards an ideal technique for cloning PCR fragments. *Nucleic*
883   *Acids Res* 34**,** e122.

884   Nørholm, M.H. (2010). A mutant Pfu DNA polymerase designed for advanced uracil-excision DNA
885   engineering. *BMC Biotechnology* 10**,** 21.

886   Olszewski, N., Sun, T.-P., and Gubler, F. (2002). Gibberellin signaling: biosynthesis, catabolism, and
887   response pathways. *The Plant cell* 14 Suppl**,** S61-S80.

888   Parker, J.L., and Newstead, S. (2014). Molecular basis of nitrate uptake by the plant nitrate
889   transporter NRT1.1. *Nature* 507**,** 68-72.

890   Pei, J., Kim, B.-H., and Grishin, N.V. (2008). PROMALS3D: a tool for multiple protein sequence
891   and structure alignments. *Nucleic acids research* 36**,** 2295-2300.

892   Plackett, A.R., Thomas, S.G., Wilson, Z.A., and Hedden, P. (2011). Gibberellin control of stamen
893   development: a fertile field. *Trends Plant Sci* 16**,** 568-578.

894   Regnault, T., Davière, J.-M., Wild, M., Sakvarelidze-Achard, L., Heintz, D., Carrera Bergua, E.,
895   Lopez Diaz, I., Gong, F., Hedden, P., and Achard, P. (2015). The gibberellin precursor GA12
896   acts as a long-distance growth signal in Arabidopsis. *Nature Plants* 1**,** 15073.

897   Regnault, T., Daviere, J.M., and Achard, P. (2016). Long-distance transport of endogenous
898   gibberellins in Arabidopsis. *Plant Signal Behav* 11**,** e1110661.

899 Rubery, P.H., and Sheldrake, A.R. (1973). Effect of pH and surface charge on cell uptake of auxin.
900   *Nat New Biol* 244**,** 285-288.

901 Saito, H., Oikawa, T., Hamamoto, S., Ishimaru, Y., Kanamori-Sato, M., Sasaki-Sekimoto, Y.,
902   Utsumi, T., Chen, J., Kanno, Y., Masuda, S., Kamiya, Y., Seo, M., Uozumi, N., Ueda, M.,
903   and Ohta, H. (2015). The jasmonate-responsive GTR1 transporter is required for gibberellin-
904   mediated stamen development in Arabidopsis. *Nat Commun* 6.

905 Sali, A., and Blundell, T.L. (1993). Comparative protein modelling by satisfaction of spatial
906   restraints. *J Mol Biol* 234**,** 779-815.

907 Segonzac, C., Boyer, J.C., Ipotesi, E., Szponarski, W., Tillard, P., Touraine, B., Sommerer, N.,
908   Rossignol, M., and Gibrat, R. (2007). Nitrate efflux at the root plasma membrane:
909   identification of an Arabidopsis excretion transporter. *Plant Cell* 19**,** 3760-3777.

910 Seki, M., Carninci, P., Nishiyama, Y., Hayashizaki, Y., and Shinozaki, K. (1998). High-efficiency
911   cloning of Arabidopsis full-length cDNA by biotinylated CAP trapper. *Plant J* 15**,** 707-720.

912 Seki, M., Narusaka, M., Kamiya, A., Ishida, J., Satou, M., Sakurai, T., Nakajima, M., Enju, A.,
913   Akiyama, K., Oono, Y., Muramatsu, M., Hayashizaki, Y., Kawai, J., Carninci, P., Itoh, M.,
914   Ishii, Y., Arakawa, T., Shibata, K., Shinagawa, A., and Shinozaki, K. (2002). Functional
915   Annotation of a Full-Length Arabidopsis cDNA Collection. *Science* 296**,** 141-145.

916 Shani, E., Weinstain, R., Zhang, Y., Castillejo, C., Kaiserli, E., Chory, J., Tsien, R.Y., and Estelle, M.
917   (2013). Gibberellins accumulate in the elongating endodermal cells of Arabidopsis root.
918   *Proceedings of the National Academy of Sciences of the United States of America* 110**,** 4834-
919   4839.

920 Solcan, N., Kwok, J., Fowler, P.W., Cameron, A.D., Drew, D., Iwata, S., and Newstead, S. (2012).
921   Alternating access mechanism in the POT family of oligopeptide transporters. *Embo j* 31**,**
922   3411-3421.

923 Sun, J., Bankston, J.R., Payandeh, J., Hinds, T.R., Zagotta, W.N., and Zheng, N. (2014). Crystal
924   structure of the plant dual-affinity nitrate transporter NRT1.1. *Nature* 507**,** 73-77.

925 Sun, T.P. (2008). Gibberellin metabolism, perception and signaling pathways in Arabidopsis.
926   *Arabidopsis Book* 6**,** e0103.

927 Tal, I., Zhang, Y., Jøgensen, M.E., Pisanty, O., Barbosa, I.C.R., Zourelidou, M., Regnault, T.,
928   Crocoll, C., Erik Olsen, C., Weinstain, R., Schwechheimer, C., Halkier, B.A., Nour-Eldin,
929   H.H., Estelle, M., and Shani, E. (2016). The Arabidopsis NPF3 protein is a GA transporter.
930   *Nat Commun* 7.

931 Tsay, Y.-F., Schroeder, J.I., Feldmann, K.A., and Crawford, N.M. (1993). The herbicide sensitivity
932   gene CHL1 of arabidopsis encodes a nitrate-inducible nitrate transporter. *Cell* 72**,** 705-713.

933 Van Westen, G.J., Swier, R.F., Cortes-Ciriano, I., Wegner, J.K., Overington, J.P., Ijzerman, A.P.,
934   Van Vlijmen, H.W., and Bender, A. (2013). Benchmarking of protein descriptor sets in
935   proteochemometric modeling (part 2): modeling performance of 13 amino acid descriptor
936   sets. *J Cheminform* 5**,** 42.

937 Wang, Y.-Y., Cheng, Y.-H., Chen, K.-E., and Tsay, Y.-F. (2018). Nitrate Transport, Signaling, and
938   Use Efficiency. *Annual Review of Plant Biology* 69**,** 85-122.

939 Wang, Y.Y., and Tsay, Y.F. (2011). Arabidopsis nitrate transporter NRT1.9 is important in phloem
940   nitrate transport. *Plant Cell* 23**,** 1945-1957.

941   Yamaguchi, S. (2008). Gibberellin metabolism and its regulation. *Annu Rev Plant Biol* 59**,** 225-251.

942